Supporting Information: Artificial Metalloproteins with Dinuclear Iron-Hyroxido Centers

Kelsey R. Miller,[§] Saborni Biswas,[⊥] Andrew Jasniewski,[†] Alec H. Follmer,[§] Ankita Biswas,[§] Therese Albert,[‡] Sinan Sabuncu,[‡] Emile L. Bominaar,[⊥] Michael P. Hendrich,[⊥]* Pierre Moënne-Loccoz,[¶]* A.S. Borovik[§]*

[§]Department of Chemistry, 1102 Natural Sciences II, University of California, Irvine, California 92697 USA

[†]Department of Molecular Biology and Biochemistry, University of California, Irvine, California 92697 USA

[⊥]Department of Chemistry, Carnegie Mellon University, 4400 Fifth Avenue, Pittsburgh, Pennsylvania 15213 USA

[‡]Department of Biochemistry and Molecular Biology, Oregon Health & Science University, Mail Code HRC3, 3181 SW Sam Jackson Park Road, Portland, Oregon 97239 USA

Table of Content

Experimental Details

General Methods. All commercially available reagents were obtained in the highest purity and used as received. Ethanol (EtOH) and diethyl ether were degassed with argon and dried by vacuum filtration through activated alumina according to the procedure by Grubbs.[1] Triethylamine was distilled from KOH. Thin-layer chromatography (TLC) was performed on Merck 60 F254 aluminum-backed silica plates or Merck 60 F254 glass-backed basic aluminum oxide plates. Eluted plates were visualized using UV light. Silica or basic alumina gel chromatography was performed with the indicated solvent system using Fisher reagent silica gel 60 (230-400 mesh) or Sigma reagent Brockmann 1 basic aluminum oxide 58 (150 mesh). Biotin pentafluorophenol ester (biot-PFP)[2] and di-(2-picolyl)amine[3] were prepared according to literature procedures. The ligand biot-et-dpa and Fe^{III} complex $[Fe^{III}(\text{biot-et-dpa})(OH_2)_3]Cl_3$ were prepared as previously described.[4]

Physical Methods

Instrumentation. ^{1}H NMR spectra were recorded at 500 MHz. ^{1}H NMR spectra were reported in ppm on the δ scale and referenced to tetramethylsilane or solvent residual. The data are presented as follows: chemical shift, multiplicity (s = singlet, d = doublet, t = triplet, q = quartet, quin = quintet, m = multiplet, br = broad), and integration. Mass spectra were measured on a MicroMass AutoSpec E, a MicroMass Analytical 7070E, or a MicroMass LCT Electrospray instrument. Electronic absorbance spectra were recorded with a Cary 50 or 8453 Agilent UV-vis spectrophotometer. X-band (9.64 GHz and 9.32 GHz) EPR spectra were recorded on a Bruker spectrometer equipped with Oxford liquid helium cryostats. The quantification of all signals was performed relative to a CuEDTA spin standard. The concentration of the standard was derived from an atomic absorption standard (Aldrich). For all instruments, the microwave frequency was calibrated with a frequency counter and the magnetic field with an NMR gaussmeter. A modulation frequency of 100 kHz was used for all EPR spectra. The EPR simulation software (SpinCount) was written by our

collaborating author, Michael P. Hendrich.[5] Mössbauer spectra were recorded with a Janis Research Super-Varitemp dewar. Isomer shifts are reported relative to Fe metal at 298 K.

Preparative Methods

2-(2-(bis(pyridin-2-ylmethyl)amino)propyl)isoindoline-1,3-dione.[4] Dpa (2.03 g, 10.0 mmol), *N*-(2-bromopropyl)phthalimide (3.00 g, 11.1 mmol), KI (0.34 g, 2.04 mmol) and K_2CO_3 (5.6 g, 41 mmol) were dissolved in 40 mL CH_3CN and refluxed for 24 h. The solution was cooled to room temperature, filtered, and reduced to dryness. The maroon-brown residue was dissolved in 30 mL DCM and washed with 3 x 30 mL aqueous $NaHCO_3$ (with a small addition of brine) and 2 x 30 mL water. The maroon-brown organic layer was acidified with 35 mL 12 mM HCl dissolved in 10 mL water and washed with 5 x 50 mL DCM. The aqueous layer was carefully neutralized with solid $NaHCO_3$ and extracted with 4 x 50 mL DCM. The solution was dried with $MgSO_4$, filtered, and reduced to dryness to yield a reddish, brown oil. The crude product was purified via column chromatography with silica gel and CH_3OH:DCM (0.5:9.5) as the eluent to yield pure product as a yellow oil (1.97 g, 48%). ^1H (500 mHz, $CDCl_3$) δ 8.48 (d, 2H), 7.82 (dd, 2H), 7.71 (dd, 2H) 7.63 (t, 2H), 7.54 (d, 2H), 7.11 (t, 2H), 3.85 (m, 4H), 3.70 (t, 2H), 2.63 (t, 2H), 1.91 (m, 4H). MS (ESI, MeOH) m/z calcd $C_{23}H_{22}N_4O_2$ [M + (H^+)] 386.17, found 386.92.

***N,N*-bis(pyridin-2-ylmethyl)propane-1,2-diamine**.[4] Hydrazine monohydrate (0.37 mL, 7.56 mmol) and **2-(2-(bis(pyridin-2-ylmethyl)amino)propyl)isoindoline-1,3-dione** (0.59 g, 1.53 mmol) were dissolved in 20 mL EtOH and refluxed under N_2 for 3 h. The phthalhydrazide byproduct precipitated as a white solid after 15 min of reflux. The solution was filtered to remove the phthalhydrazide and washed with 3 x 10 mL chloroform. The solution was reduced to dryness, and the yellow oily residue was dissolved in 20 mL $CHCl_3$ and 20 mL of 1 M NaOH. The aqueous layer was extracted with 3 x 20 mL $CHCl_3$, dried over $MgSO_4$, filtered, and reduced to dryness. The product was recovered as a yellow oil (0.21 g, 55%). ^1H (500 mHz, $CDCl_3$) δ 8.53 (d, 2H), 7.65 (t,

2H), 7.52 (d, 2H) 7.14 (t, 2H), 3.81 (s, 4H), 2.70 (t, 2H), 2.60 (t, 2H), 1.68 (q, 2H). MS (ESI, MeOH) m/z calcd $C_{15}H_{20}N_4$ [M + (Na^+)] 279.16, found 279.14.

biot-pr-dpa.[4] A solution of biot-PFP (0.31 g, 0.76 mmol), *N*,*N*-bis(pyridin-2-ylmethyl)propane-1,2-diamine (0.21 g, 0.82 mmol), and triethylamine (0.09 g, 0.89 mmol) in 10 mL DMF was stirred overnight. The DMF was removed under vacuum to yield a sticky tan residue. The residue was triturated with diethyl ether until a free-flowing solid formed (3-7 days). The light tan solid was filtered, washed with diethyl ether, and dried under vacuum. The solid was stored under an inert atmosphere (0.33 g, 83%). ^{1}H (500 mHz, DMSO) δ 8.48 (d, 2H), 7.77 (br, 1H), 7.75 (t, 2H) 7.50 (d, 2H), 7.25 (t, 2H), 6.42 (s, 1H), 6.35 (s, 1H), 4.31 (t, 1H), 4.11 (t, 1H), 3.71 (s, 4H), 3.03 (m, 1H), 3.01 (q, 2H), 2.81 (dd, 1 H), 2.57 (d, 1 H), 2.46 (t, 1H), 2.46 (s, 2H), 2.00 (t, 2H), 1.62 (m, 8H). MS (ESI, MeOH) m/z calcd $C_{25}H_{34}N_6O_2S$ [M + (Na^+)] 505.24, found 505.17.

2-(2-(bis(pyridin-2-ylmethyl)amino)butyl)isoindoline-1,3-dione.[4] Dpa (2.02 g, 10.1 mmol), *N*-(2-bromobutyl)phthalimide (3.15 g, 11.2 mmol), KI (0.34 g, 2.03 mmol) and K_2CO_3 (6.1 g, 44 mmol) were dissolved in 40 mL CH_3CN and refluxed for 24 h. The solution was cooled to room temperature, filtered, and reduced to dryness. The maroon-brown residue was dissolved in 50 mL DCM and washed with 3 x 50 mL aqueous $NaHCO_3$ (with a small addition of brine) and 2 x 30 mL water. The maroon-brown organic layer was acidified with 40 mL 12 mM HCl dissolved in 20 mL water and washed with 5 x 50 mL DCM. The aqueous layer was carefully neutralized with solid $NaHCO_3$ and extracted with 4 x 50 mL DCM. The solution was dried with $MgSO_4$, filtered, and reduced to dryness to yield a reddish, brown oil. The crude product was purified via column chromatography with silica gel and CH_3OH:DCM (0.5:9.5) as the eluent to yield pure product as a yellow oil (1.35 g, 31%). Note: column chromatography is not necessary for purification if the extractions are completed efficiently. ^{1}H (500 mHz, $CDCl_3$) δ 8.49 (d, 2H), 7.82 (dd, 2H), 7.71 (dd,

2H) 7.63 (t, 2H), 7.53 (d, 2H), 7.12 (t, 2H), 3.79 (m, 4H), 3.63 (t, 2H), 2.57 (t, 2H), 1.67 (m, 2H), 1.57 (m, 2H). MS (ESI, MeOH) *m/z* calcd $C_{24}H_{24}N_4O_2$ [M + (H^+)] 401.2, found 401.3.

***N*,*N*-bis(pyridin-2-ylmethyl)butane-1,2-diamine**.[4] Hydrazine monohydrate (0.74 mL, 15.2 mmol) and **2-(2-(bis(pyridin-2-ylmethyl)amino)butyl)isoindoline-1,3-dione** (1.22 g, 3.05 mmol) were dissolved in 50 mL EtOH and refluxed under N_2 for 3 h. The phthalhydrazide byproduct precipitated as a white solid after 15 min of reflux. The solution was filtered to remove the phthalhydrazide and washed with 3 x 10 mL chloroform. The solution was reduced to dryness, and the yellow oily residue was dissolved in 20 mL $CHCl_3$ and 20 mL of 1 M NaOH. The aqueous layer was extracted with 3 x 20 mL $CHCl_3$, dried over $MgSO_4$, filtered, and reduced to dryness. The product was recovered as a yellow oil (0.50 g, 60%). ^{1}H (500 mHz, $CDCl_3$) δ 8.52 (d, 2H), 7.65 (t, 2H), 7.52 (d, 2H) 7.14 (t, 2H), 3.81 (s, 4H), 2.62 (t, 2H), 2.55 (t, 2H), 1.57 (m, 2H), 1.41 (m, 2H), 1.41 (br, 2H). MS (ESI, MeOH) *m/z* calcd $C_{16}H_{22}N_4$ [M + (H^+)] 271.2, found 271.4.

biot-bu-dpa.[4] A solution of biot-PFP (0.69 g, 1.68 mmol), *N*,*N*-bis(pyridin-2-ylmethyl)butane-1,2-diamine (0.50 g, 1.85 mmol), and triethylamine (0.20 g, 2.02 mmol) in 20 mL DMF was stirred overnight. The DMF was removed under vacuum to yield a sticky tan residue. The residue was triturated with diethyl ether until a free-flowing solid formed (3-7 days). The light tan solid was filtered, washed with diethyl ether, and dried under vacuum. The solid was stored under an inert atmosphere (0.46 g, 50%). ^{1}H (500 mHz, DMSO) δ 8.47 (d, 2H), 7.77 (br, 1H), 7.75 (t, 2H) 7.51 (d, 2H), 7.25 (t, 2H), 6.40 (s, 1H), 6.34 (s, 1H), 4.29 (t, 1H), 4.11 (t, 1H), 3.70 (s, 4H), 3.07 (m, 2H), 2.97 (q, 1 H), 2.78 (dd, 1 H), 2.57 (d, 1H), 2.43 (t, 2H), 2.03 (t, 2H), 1.33 (m, 10H). MS (ESI, MeOH) *m/z* calcd $C_{26}H_{36}N_6O_2S$ [M + (Na^+)] 519.18, found 519.19.

Preparation of Metal Complexes

[Fe^{III}(biot-pr-dpa)(OH_2)$_3$]Cl_3.[4] [Fe^{III}(biot-pr-dpa)(OH_2)$_3$]Cl_3 was prepared according to literature procedure to yield a yellow solid (0.10 g, 77%). HRMS (ESI, MeOH) *m/z* calcd for

$C_{27}H_{40}Cl_2FeN_6O_2S$ [M – ($3Cl^-$) + $(OCH_3)_2$] 600.22, found 600.21. Elem. Anal. Calcd for ($C_{25}H_{40}N_6SO_5FeCl_3$): C, 42.96; H, 5.77; N, 12.03. Found: C, 42.56; H, 5.07; N, 11.89.

[Fe^{III}(biot-bu-dpa)$(OH_2)_3$]Cl_3.[4] [Fe^{III}(biot-bu-dpa)$(OH_2)_3$]Cl_3 was prepared according to literature procedure to yield a yellow solid (0.11 g, 96%). HRMS (ESI, MeOH) *m/z* calcd for $C_{28}H_{42}Cl_2FeN_6O_2S$ [M – ($3Cl^-$) + $(OCH_3)_2$] 614.23, found 614.21. Elem. Anal. Calcd for ($C_{26}H_{42}N_6SO_5FeCl_3$): C, 43.80; H, 5.94; N, 11.79. Found: C, 43.69; H, 5.49; N, 11.65.

Sample Preparations for Spectroscopic Studies

HABA Titrations. To 2.4 mL of 8 μM S_{112}Y-Sav, K_{121}Y-Sav, or K_{121}A-L_{124}Y-Sav in 200 mM sodium phosphate buffer at pH 7 was added 300 μL of a 10 mM 2-(4'-hydroxyazobenzene)benzoic acid (HABA) solution in 200 mM phosphate buffer pH 7. After 5 min of equilibration, the absorbance at 506 nm was recorded. A solution of 1 mM Fe complex in nanopure water was added in 4-20 μL portions until approximately 4 equivalents of the appropriate Fe complex had been added. The absorbance at 506 nm was recorded until no further changes in intensity were observed.

Preparation of Proteins

Protein Expression and Purification

Preparation of Sav Variants. The construction of K_{121}A-L_{124}Y-Sav and other variants was achieved by site-directed mutagenesis (SDM) using the codon optimized K_{121}A-pET24a-Sav plasmid,[12] the following primers and, and Q5 polymerase.

L_{124}Y_fwd: 5'-CAGCACCTATGTTGGTCATGATACCTTTC-3'

L_{124}Y_rev: 5'-CACCAACATAGGTGCTTTTCCAGGCATTC-3'

Amplification of pET24a-Sav mutant plasmids was accomplished by the transformation of SDM reaction mixtures into DH5α ultracompetent cells. Plasmids were isolated using a Miniprep kit from Qiagen, eluting the final plasmid with distilled deionized-water (ddH_2O, 18 MΩ cm^{-1}). DNA sequencing was performed by Genewiz.

Expression of Sav Variants. Transformation of 4 µL amplified plasmids into 50 µL Rosetta cells or bl21 cells was followed by rescue with 450 µL LB media. Of this solution, 200 µL was spread aseptically onto LB/Kanamycin agar plates and incubated overnight at 37 °C. Inoculation of a starter culture containing 500 mL LB media and the same antibiotic from a single colony was followed by incubation overnight at 37 °C and shaking at 225 rpm. From this starter culture, 25 mL was used to inoculate each 2L flask containing 500 mL LB media, 25 mL each of 20x sugar (12% glycerol, 1% glucose, 10% lactose) and salt (1 M Na_2HPO_4, 1 M KH_2PO_4, 0.5 M $(NH_4)_2SO_4$) stocks, 1 mL of 1 M $MgSO_4$, 100 µL 5000x trace metal mix (containing 1 M $CaCl_2$, 100 mM $FeCl_3$, 10 mM $MnCl_2$, 10 mM $ZnSO_4$, 2 mM $CoCl_2$, 2 mM $CuCl_2$, 2 mM $NiCl_2$, 2 mM Na_2MoO_4, and 2 mM H_3BO_3 all in 60 mM HCl), and 250 µL of 100 mg/mL Kanamycin. Incubation at 37 °C and 225 rpm was continued until cells reached OD_{600} = 0.6–0.8, at which point the temperature was dropped to 25 °C and cultures incubated another 24 h.

Purification of Sav Variants. Cultures were centrifuged at 4000 x *g* for 20 min at 4 °C. The resulting cell pellet was resuspended in lysis buffer (50 mL per 1 L expressed) containing 20 mM Tris buffer pH 7.4, 1 mg/mL lysozyme, and a spatula tip of DNase I. The suspension was then allowed to shake at 25 °C and 225 rpm for 6-8 h followed by one overnight freeze-thaw cycle. Dialysis against 6 M guanidinium hydrochloride pH 1.5 for 24 h was followed by neutralization via dialysis against 20 mM Tris buffer pH 7.4 for 24 h, and against nanopure H_2O for another 24 h. Dialysis overnight against iminobiotin (IB) buffer containing 500 mM NaCl and 50 mM $NaHCO_3$ at pH 10.5 afforded the crude, biotin-free lysate that was centrifuged at 10,000 x *g* for 1 h at 4 °C, and the soluble portion loaded onto an iminobiotin-agarose column pre-equilibrated with IB buffer. The column was washed with 6 column volumes (CVs) of IB buffer or until the absorbance at 280 nm (A_{280}) dropped to zero. Elution with 1% acetic acid in nanopure H_2O, and pooling fractions by A_{280}, provided highly pure (>95%) Sav as assessed by 18% SDS-PAGE. Pooled fractions were dialyzed against 10

mM Tris pH 7.4 for 24 h followed by dialysis in ddH_2O for an additional 72 h and were then lyophilized. Yields of lyophilized protein were typically 100 mg per L expressed, and the solid protein was stored at 4 °C.

Sample Preparations

Electronic Absorption Studies. General Procedure: A solution of lyophilized S_{112}Y-Sav, K_{121}Y-Sav, or K_{121}A-L_{124}Y-Sav (50-250 μM) was prepared in nanopure water. Four equivalents of Fe complex (0.2-1 mM) in nanopure water were added to the protein solution. Samples were prepared in a final volume of 500 μL with nanopure water. It is **important** to note that all solution experiments had to be performed in nanopure water in the absences of buffer. (Note, it is know that Sav is stable in water without buffers).[ref] Addition of a buffer (e.g., Good's, phosphate, >100 mM acetate) or organic solvents (e.g., DMF) appears to disrupt the Fe–phenolate interaction and the characteristic blue color of **1** was not observed.

EPR Spectral Studies. A solution of K_{121}A-L_{124}Y-Sav (500 μM) was prepared in nanopure water. Four equivalents of Fe complex (2 mM) in nanopure water were added to the protein solution. Samples were prepared to a final volume of 200 μL by the addition of nanopure water. The sample was transferred to an EPR tube and frozen at 77 K.

Mössbauer Spectral Studies. A solution of K_{121}A-L_{124}Y-Sav (500 μM) was prepared in nanopure water. Four equivalents of Fe complex (2 mM) in nanopure water were added to the protein solution. Samples were prepared in a final volume of 300 μL with nanopure water. The sample was prepared in a solution Mössbauer cup, frozen at 77 K in liquid nitrogen, and run at 4 K. $^{57}Fe^{III}$ crystalline samples were prepared as described below and transferred into a solid Mossbauer cup, frozen at 77 K, and run at various temperatures.

XAS Studies. A solution of K_{121}A-L_{124}Y-Sav (750 μM) was prepared in nanopure water. Four equivalents of Fe complex (3 mM) in nanopure water were added to the protein solution. Samples

were prepared in a final volume of 250 uL with nanopure water and 30% glycerol. The sample was pipetted into a small delrin solution cell and frozen at 77 K in liquid nitrogen.

Resonance Raman Studies. A solution of K_{121}A-L_{124}Y-Sav (1.25 mM) was prepared in nanopure water. Four equivalents of Fe complex (5 mM) in nanopure water were added to the protein solution. Samples were prepared in a final volume of 300 μL with nanopure water. The sample was prepared in an Eppendorf tube, frozen at 195 K in dry ice (for shipping purposes) and run at room temperature.

Data Collection and Processing

Resonance Raman Data Collection and Processing. Resonance Raman spectra were obtained at room temperature on samples in glass capillaries (3-5 mM concentration in Fe) using a 90° geometry with a custom McPherson 2061/207 spectrograph equipped with a liquid N_2-cooled CCD detector (LN-1100PB, Princeton Instruments). The 647-nm excitation was derived from a Kr laser (Innova 302, Coherent). A long-pass filter (RazorEdge, Semrock) was used to attenuate Rayleigh scattering. Comparison of rapid acquisitions with a range of laser power and continuous sample translation with longer data acquisitions provided no evidence of photosensitivity for all the Sav samples. The integrity of the rR samples was confirmed by direct monitoring of their UV-vis absorption spectra in Raman capillaries before and after laser exposure. Frequencies were calibrated relative to indene and are accurate to ± 1 cm^{-1}. Polarization conditions were optimized using CCl_4 and indene.

XAS Data Collection, and Processing. Fe K-edge X-ray absorption spectra were collected on SSRL beam line 9-3 using a 100-element Ge monolith solid-state detector (Canberra) with a SPEAR3 storage ring current of ~500 mA at an energy of 3.0 GeV. The beam line 9-3 optics consist of a flat, bent, harmonic rejection vertically collimating Rh-coated Si M_0 mirror as well as a cylindrical, bent, Rh-coated focusing M_1 mirror. A total of six Fe K-edge scans were taken between 6882 and 8000 eV at ~10 K using an Oxford Instruments CF1208 continuous flow liquid helium cryostat using an open-cycle liquid He

dewar (BL 9-3). An Fe foil was placed in the beam pathway prior to the ionization chamber I_0 and scanned concomitantly for an energy calibration, with the first inflection point of the edge assigned to 7112.0 eV. A Soller slit with a 3 μm Mn filter was used to increase the signal to noise ratio of the spectra. Photoreduction was monitored by scanning the same spot on the sample twice and comparing the first derivative peaks associated with the edge energy during data collection.

The detector channels from the scans were examined, calibrated, averaged, and processed using EXAFSPAK.[9] Theoretical phase and amplitude parameters for a given absorber-scatterer pair were calculated using FEFF 8.40[10] and subsequently applied to the nonlinear least squares 'opt' fitting program of the EXAFSPAK package during curve fitting. Parameters for each species were calculated using an appropriate model derived from the crystal structure. In all analyses, the coordination number of a given shell (N) was a fixed parameter and was varied iteratively in integer steps, whereas the bond lengths (R) and mean-square deviation (σ^2) were allowed to freely float. The estimated uncertainties in R, σ^2, and N are 0.02 Å, 0.1 × 10^{-3} Å^2, and 20%, respectively. The amplitude reduction factor S_0 was fixed at 1.0 for the Fe K-edge data, whereas the edge-shift parameter ΔE_0 was allowed to float as a single value for all shells. Thus, in any given fit, the number of floating parameters was typically equal to 2 × number of shells + 1. The goodness of fit (GOF) parameters are calculated as follows:

$$F = \sqrt{\sum k^6 \left(\chi_{\exp} - \chi_{calc}\right)^2}$$

$$F' = \sqrt{\sum k^6 \left(\chi_{\exp} - \chi_{calc}\right)^2 / \sum k^6 \chi_{\exp}{}^2}$$

Pre-edge analysis was performed on the Fe K-edge fluorescence data normalized to have an edge jump of 1.0 at 7130 eV in the "process" program of the EXAFSPAK package. The pre-edge features were fit as described elsewhere[3] between 7108 eV to 7118 eV using the Fityk[11] program with pseudo-Voigt functions composed of 50:50 Gaussian/Lorentzian functions.

Crystallographic Methods

Protein Crystallization

*Crystallization of [Fe_2^{III}(biot-bu-dpa)$_2$(OAc)(μ–O)(O_{Y124})$_2$⊂K_{121}Y-L_{124}Y-Sav] (**1**).* Apo-Sav protein was crystallized by the sitting drop vapor diffusion method. Diffraction-quality crystals were grown at room temperature by mixing 4 μL of protein solution (26 mg/mL lyophilized protein in water) and 1 μL of crystallization buffer (2.0 ammonium sulfate, 0.1 M sodium acetate, pH 4). The droplet was equilibrated against a reservoir solution of 100 μL crystallization buffer. Single crystals of Sav were prepared by soaking apo-crystals in a soaking buffer (3.0 ammonium sulfate) with a 10 mM stock solution of [Fe^{III}(biot-bu-dpa)$(OH_2)_3$]Cl_3 in nanopure water (9 μL crystallization buffer, 1 μL [Fe^{III}(biot-bu-dpa)$(OH_2)_3$]Cl_3 overnight. After the soaking, crystals were transferred to cryo-protectant for 1 min (30% glycerol in crystallization buffer) and shock-frozen in liquid nitrogen. Crystals were prepared in a similar manner for Mossbauer studies, with the exception that $^{57}Fe^{III}$(biot-bu-dpa)$(OH_2)_3$]Cl_3 was used for soaking. Crystalline samples were prepared from harvesting multiple crystal trays (10 48-well trays) into an eppendorf tube and soaking $^{57}Fe^{III}$(biot-bu-dpa)$(OH_2)_3$]Cl_3 in a 1:9 ratio of complex to buffer overnight. The crystalline solution was then transferred with minimal solution to solid Mössbauer cups and frozen at 77 K. *An important note is that the 0.1 M sodium acetate must be removed for successfully soaking the [Fe^{III}(biot-bu-dpa)$(OH_2)_3$]Cl_3 complex into K_{121}Y-L_{124}Y-Sav. If acetate is present in the soaking step, the crystals will not turn blue.*

*Crystallization of [Fe_2^{III}(biot-bu-dpa)$_2$(μ–1,3–OAc)(μ–O)(O_{Y124})$_2$⊂K_{121}Y-L_{124}Y-Sav] (**1**–OAc).* Apo-Sav protein was crystallized by the sitting drop vapor diffusion method. Diffraction-quality crystals were grown at room temperature by mixing 4 μL of protein solution (26 mg/mL lyophilized protein in water) and 1 μL of crystallization buffer (2.0 ammonium sulfate, 0.1 M sodium acetate, pH 4). The droplet was equilibrated against a reservoir solution of 100 μL crystallization buffer. Single crystals of Sav were prepared by soaking apo-crystals in a soaking buffer (3.0 ammonium sulfate) with a 10

mM stock solution of $[Fe^{III}(biot\text{-}bu\text{-}dpa)(OH_2)_3]Cl_3$ in nanopure water (9 μL crystallization buffer, 1 μL $[Fe^{III}(biot\text{-}bu\text{-}dpa)(OH_2)_3]Cl_3$ overnight. Once the crystals turned blue, they were soaked in the soaking buffer (3 M ammonium sulfate) with a 1 M stock of NaOAc in nanopure water for 1-5 min (9 μL soaking buffer, 1 μL NaOAc). After the second soaking, the crystals were transferred to cryo-protectant for 1 minute (30% glycerol in soaking buffer) and shock-frozen in liquid nitrogen. Crystals were prepared in a similar manner for Mossbauer studies, with the exception that $^{57}Fe^{III}(biot\text{-}bu\text{-}dpa)(OH_2)_3]Cl_3$ was used for soaking. Crystalline samples were prepared from harvesting multiple crystal trays (10 48-well trays) into an eppendorf tube and soaking $^{57}Fe^{III}(biot\text{-}bu\text{-}dpa)(OH_2)_3]Cl_3$ in a 1:9 ratio of complex to buffer overnight. The crystalline solution was then transferred with minimal solution to solid Mössbauer cups and frozen at 77 K.

Crystallization of $[Fe_2^{III}(biot\text{-}bu\text{-}dpa)_2(\mu\text{–}1,3\text{–}N_3)(\mu\text{–}O)(O_{Y124})_2 \subset K_{121}Y\text{-}L_{124}Y\text{-}Sav$ (***1***$\text{–}N_3)]$. Apo-Sav protein was crystallized by the sitting drop vapor diffusion method. Diffraction-quality crystals were grown at room temperature by mixing 4 μL of protein solution (26 mg/mL lyophilized protein in water) and 1 μL of crystallization buffer (2.0 ammonium sulfate, 0.1 M sodium acetate, pH 4). The droplet was equilibrated against a reservoir solution of 100 μL crystallization buffer. Single crystals of Sav were prepared by soaking apo-crystals in a soaking buffer (3.0 ammonium sulfate) with a 10 mM stock solution of $[Fe^{III}(biot\text{-}bu\text{-}dpa)(OH_2)_3]Cl_3$ in nanopure water (9 μL crystallization buffer, 1 μL $[Fe^{III}(biot\text{-}bu\text{-}dpa)(OH_2)_3]Cl_3$ overnight. Then, the crystals were soaked in the soaking buffer (3 M ammonium sulfate) with a 1 M stock of NaN_3 in nanopure water for 1-5 min (9 μL soaking buffer, 1 μL NaOAc). After the second soaking, the crystals were transferred to cryo-protectant for 1 minute (30% glycerol in soaking buffer) and shock-frozen in liquid nitrogen.

Crystallization of $[Fe_2^{III}(biot\text{-}bu\text{-}dpa)_2(\mu\text{–}1,3\text{–}SCN)(\mu\text{–}O)(O_{Y124})_2 \subset K_{121}Y\text{-}L_{124}Y\text{-}Sav$ (***1***$\text{–}CN)]$. Apo-Sav protein was crystallized by the sitting drop vapor diffusion method. Diffraction quality crystals were grown at room temperature by mixing 4 μL of protein solution (26 mg/mL lyophilized protein in

water) and 1 μL of crystallization buffer (2.0 ammonium sulfate, 0.1 M sodium acetate, pH 4). The droplet was equilibrated against a reservoir solution of 100 μL crystallization buffer. Single crystals of Sav were prepared by soaking apo-crystals in a soaking buffer (3.0 ammonium sulfate) with a 10 mM stock solution of $[Fe^{III}(biot\text{-}bu\text{-}dpa)(OH_2)_3]Cl_3$ in nanopure water (9 μL crystallization buffer, 1 μL $[Fe^{III}(biot\text{-}bu\text{-}dpa)(OH_2)_3]Cl_3$ overnight. Then, the crystals were soaked in the soaking buffer (3 M ammonium sulfate) with a 1 M stock of NaCN in nanopure water for 1-5 min (9 μL soaking buffer, 1 μL NaOAc). After the second soaking, the crystals were transferred to cryo-protectant for 1 minute (30% glycerol in soaking buffer) and shock-frozen in liquid nitrogen.

X-ray diffraction data collection processing. X-ray diffraction data were collected at the Stanford Synchrotron Radiation Lightsource (BL 12.2) and the Advanced Light Source (BL 5.0.2. and 8.2.1) at a wavelength of 1 Å. Data were collected with helical (SSRL) or vector (ALS) data collection using exposure time/frame 0.2/0.2 s/deg or 0.5/1 s/deg. Helical or vector collection was used because it minimized the amount of radiation damage on the crystal, which ensures better quality data and limited photoreduction. Additionally, using these collection techniques helps ensure that the exogenous ligands are not dissociated during the collection time. X-ray diffraction data were processed with XDS[13] or iMosflm and scaled with AIMLESS (CCP4 Suite). The structures were solved by molecular replacement using program PHASER (CCP4 Suite) and the structure 2QCB from the PDB as input model ligand with water molecules removed. For structure refinement, REFMAC5 (CCP4 Suite) and PHENIX.REFINE were used. Ligand manipulation was carried out with program REEL using the small molecule crystal structure RAGQEV01 from the Cambridge Structural Database as an input model. For water picking, electron density, and structure visualization, the software COOT[14] was used. Figures were drawn with PyMOL (the PyMOL Molecular Graphics System, Version 1.8.2.3, Schrödinger, LLC). Crystallographic details, processing and refinement statistics are given in Supplementary Table 4.2-4.7.

Structural Results

Crystal Color. All crystals of Sav soaked with the complex $[Fe^{III}(biot\text{-}bu\text{-}dpa)(OH_2)_3]Cl_3$ changed from colorless to dark blue. Crystals soaked with NaOAc remained dark blue. Crystals soaked with NaN_3 changed from dark blue to dark red. Crystals soaked with NaCN changed to a purple-blue color.

Structural Refinement. Apo-crystals of proteins $K_{121}A\text{-}L_{124}Y$-Sav soaked with $[Fe^{III}(biot\text{-}bu\text{-}dpa)(OH_2)_3]Cl_3$ constituted space group $I4_122$ with unit cell parameters reported in Tables S4 and S15. A single Sav monomer was obtained per asymmetric unit after molecular replacement. Protein residues 2-10 and 135-159 of the N- and C-terminus, respectively, were not resolved in the electron density, presumably due to disorder. Starting from the Sav monomer, the biological homotetramer is generated by application of crystallographic C_2-symmetry axes along the x-, y- and z-axes of the unit cell. The overall protein structures are virtually identical to structure biotin ⊂ WT-Sav (PDB 1STP, see Tables S4 and S6). Because the crystallographic C_2-symmetry axis lies directly at the interface where the two monomers of Sav connect, the apo-crystals of proteins $K_{121}A\text{-}L_{124}Y$-Sav soaked with $[Fe^{III}(biot\text{-}bu\text{-}dpa)(OH_2)_3]Cl_3$ were also solved in reduced C121 symmetry to ensure that the bridging atoms were not artifacts of symmetry. The unit cell parameters are reported in Tables S6 and S15 4.4 and 4.6. A single Sav tetramer was obtained per asymmetric unit after molecular replacement.

General Complex Modeling. For all structures of apo-protein crystals soaked with the corresponding Fe-complexes, the following general observations were made: i) residual electron density in the F_o-F_c map was observed in the biotin binding pocket, ii) the biotin vestibule is flanked by protein residues of loop-3,4^A (the superscript number indicates Sav monomer within tetramer) loop-4,5^C, loop-5,6^A loop-7,8^A and loop-7,8^B, and iii) an anomalous dispersion density map indicated a significant peak in the biotin vestibule superimposed with the electron density peak. The residual electron density was fit with the corresponding Fe-complexes, which projected Fe to the position of the strong anomalous density peak.

*Structural Refinement of **1***. In the $I4_122$ symmetry solution, the biot-bu-dpa ligand, μ-hydroxido bridging ligand, and tyrosine amino acid residues are modelled with 100% occupancy (Figure S8A, Tables S4 and S5). The Fe center is modelled with 60% occupancy due to a large amount of negative density. There are several reasons there could be negative density around the Fe center: 1) the crystal was collected at an energy of 1 Å, which is far from the 1.7 Å Fe edge energy, 2) at a higher symmetry, the Fe centers are close to the center of symmetry for the monomer of Sav, and 3) there is disorder associated with the entire chelator portion of the biotinylated complex [Fe^{III}(biot-bu-dpa)]. Due to the disorder associated with the pyridine groups of the biotinylated ligand, there could be movement of the pyridyl groups and Fe center, which would cause negative density to arise around the Fe center.

In the C121 symmetry solution (Figure S9, Tables S6 and S7), the biot-bu-dpa ligands, μ-hyroxido bridging ligand, and tyrosine amino acid residues are modelled with 100% occupancy. However, the Fe center is modelled with 80% occupancy. The increase of the occupancy of the Fe center can be possibly explained by the change in the asymmetric unit. In the lower symmetry solution, the asymmetric unit is the tetramer of Sav and there is no longer a center of symmetry between the two monomers of Sav that constitute one dimer. Without this center of symmetry, it is possible that the negative density around the Fe center lessened as it is being contributed to by the disorder of the pyridyl rings still.

*Structural Refinement of **1**–OAc*. For the solution of **1**–OAc, the biot-bu-dpa ligands, μ-hydroxido bridging ligand, Fe centers, and tyrosine amino acid residues are modelled with 100% occupancy. However, there is a discrepancy between the $I4_122$ and the C121 symmetry solutions (Figures S8B and S10, Tables S4-S7). In the higher symmetry structure, the μ-hydroxido bridging ligand is fit with 100% occupancy. In contrast, in the lower symmetry solution, the resolved structure revealed that one Sav dimer had all the components found at higher symmetry that included the acetate and μ-

hydroxido bridging ligand. In the other Sav dimer, all the components found at higher symmetry were present at similar distances and angles except the μ-hydroxido bridging ligand which was missing. When solving this molecular structure with at lower symmetry (C121) the resolution of the structure is decreased (1.50 to 1.65 Å). One possible reason for the missing density of the μ-hydroxido bridging ligand is because there is not sufficient resolution to observe this denisty. With the bond distances of the di-Fe active site remaining similar between the two dimers, this lower resolution is a likely reason for the discrepancy between the structures solved in two different space groups. To test this premise, two solutions were attempted to determine if the occupancy of the μ-hydroxido bridging ligand was assigned correctly. In the higher symmetry solution (the $I4_122$ structures), the symmetry mate of the monomer reveals that the bridging ligands are in the same x,y,z coordinates as the solved structure. For this reason, the occupancy is initially decreased to 50% when solving $I4_122$ structures. Then in the $I4_122$ symmetry solution, the occupancy of the μ-hydroxido bridging ligand was decreased from 50% to 25%. The solution gave more density in the F_o-F_c map, indicating that the occupancy was incorrect at 25%. In the C121 symmetry, the occupancy was decreased from 100% to 50% for the μ-hydroxido bridging ligand. At this lower occupancy, the solution showed no F_o-F_c density for the one of the μ-hydroxido bridging ligand in one dimer and gave more density in the F_o-F_c map in the dimerwith the μ-hydroxido bridging ligand. This result indicates that lowering the occupancy of the μ-hydroxido bridging ligand did not have any effect on the density of the missing μ-hydroxido bridging ligand and that the assignment for the 100% occupancy is correct. With the results from the two occupancy tests, it is possible that the μ-hydroxido bridging ligand density is not present because of resolution restraints.

Structural Refinement of ***1***–N_3. For the solution of **1**–N_3, the biot-bu-dpa ligands, μ-hydroxido bridging ligand, Fe centers, and tyrosine amino acid residues are modelled with 100% occupancy. However, there is a discrepancy in bond distances to the azido bridging ligand between the $I4_122$ and C121

symmetry solutions (Figures S8C and S13, Tables S4-S7). In the $I4_122$ symmetry solution, the Fe–N4 bond distance between is 2.45 Å; however, in the C121 symmetry solution, the average Fe–N4 bond distance is 2.32 Å. One possible reason for the 0.13 Å difference in bond distance is because the azido ligand is located at the center of symmetry in the $I4_122$ symmetry solution. It is difficult to determine accurate bond distances when a ligand lies directly on a center of symmetry because of symmetry artifacts in the F_o-F_c map[References needed] Additionally, there is density above the azido ligand that is present up to ~5 σ in the F_o-F_c map. Attempts to model this extra density with the azido ligand adopting another conformation were unsuccessful. For example, the azido ligand was modelled as binding to only one Fe center rather than bridging between the Fe centers within the Sav dimer. All attempts to fit this possibility resulted in increased density in the F_o-F_c map around the bridging azido ligand and negative density around the second conformation of the azido ligand. Additionally, the position of the bridging azido ligand would change and fits to the $2F_o$-F_c density were substantially poorer when including the conformation of the second azido ligand. We also considered whether an acetate ion was coordinated to the Fe centers in **1**-N_3; however, similar results were determined as discussed above. If there is an additional ligand present that fits the F_o-F_c density well, that ligand is likely to only minor occupancy (less than 5%).

*Structural refinement of **1**–CN*. For the solution of **1**–CN, the biot-bu-dpa ligands, μ-hydroxido bridging ligand, Fe centers, and tyrosine amino acid residues are modelled with 100% occupancy. For both the $I4_122$ and C121 symmetry solutions, there is extra density in the F_o-F_c map above the cyanido ligand (Figures S14 and S15, Tables S15 and S16). In the $I4_122$ symmetry solution, it is possible that there is a second conformation of the cyanido ligand, where instead of bridging in a μ-(1,2) fashion to the two Fe centers, the cyanido ligand is coordinated monodentate to one Fe center. The solution of this second conformation was attempted. However, the monodentate cyanido ligands only fit the density when they are less than 1 Å apart from each other, which makes this solution chemically

unreasonable. In the C121 symmetry solution, placing the cyanido ligand bridging in a μ-(1,2) fashion between the two Fe centers matches the F_o-F_c density well and does not support a second conformation. With the C121 symmetry solution, it is possible that the second conformation of the cyanido ligand might be a symmetry artifact because there is significantly less F_o-F_c density and the cyanido ligand lies on the center of symmetry for the monomeric Sav.

Computations

DFT Calculations. The DFT calculations were performed with Gaussian 09,[15] using the density functional B3LYP and basis set 6-311G. The geometry optimizations were performed for the broken symmetry (BS) state, using default convergence criteria. Adopting the $J\mathbf{S}_1\cdot\mathbf{S}_2$ convention, the J values were calculated using the expression $J = (E_F - E_{BS})/12.5$, where E_F and E_{BS} are the electronic energies of the ferromagnetic (S = 5) and BS states, respectively, which were both evaluated for the BS optimized structure.

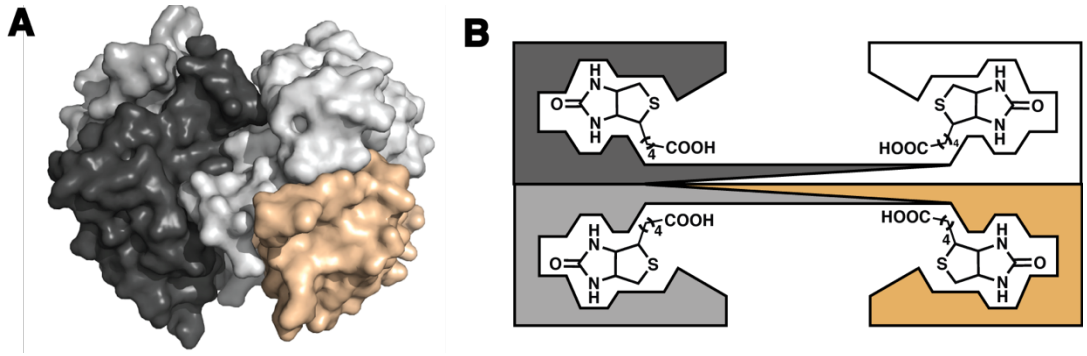

Figure S1. Surface representation of Sav (**A**) and schematic illustrating the dimer of dimer arrangement of subunits (**B**).

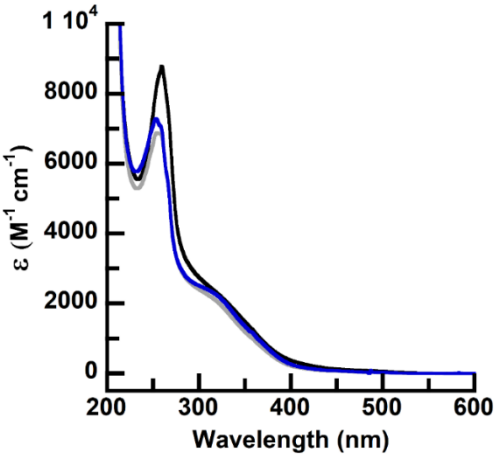

Figure S2 Electronic absorbance spectra of Fe^{III}-n-dpa collected in nanopure H_2O at RT. Key: n = 2 (black), et; 3, pr (grey); 4, bu (blue).

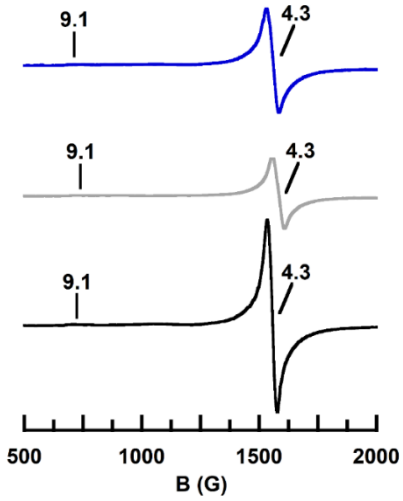

Figure S3. EPR spectra of Fe^{III}-n-dpa collected on frozen solutions at 10 K. Key: n = 2 (black), et; 3, pr (grey); 4, bu (blue).

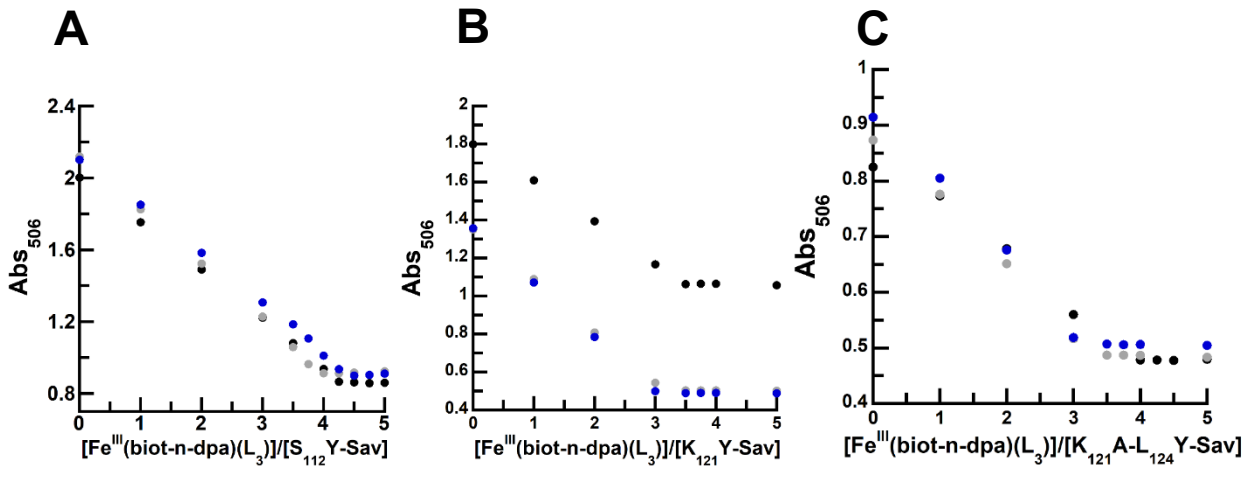

Figure S4. HABA titrations of Fe^{III}-n-dpa in S_{112}Y-Sav (**A**), K_{121}Y-Sav (**B**), and K_{121}A/L_{124}Y-Sav (**C**). n = 2 (black), et; 3, pr (grey); 4, bu (blue).

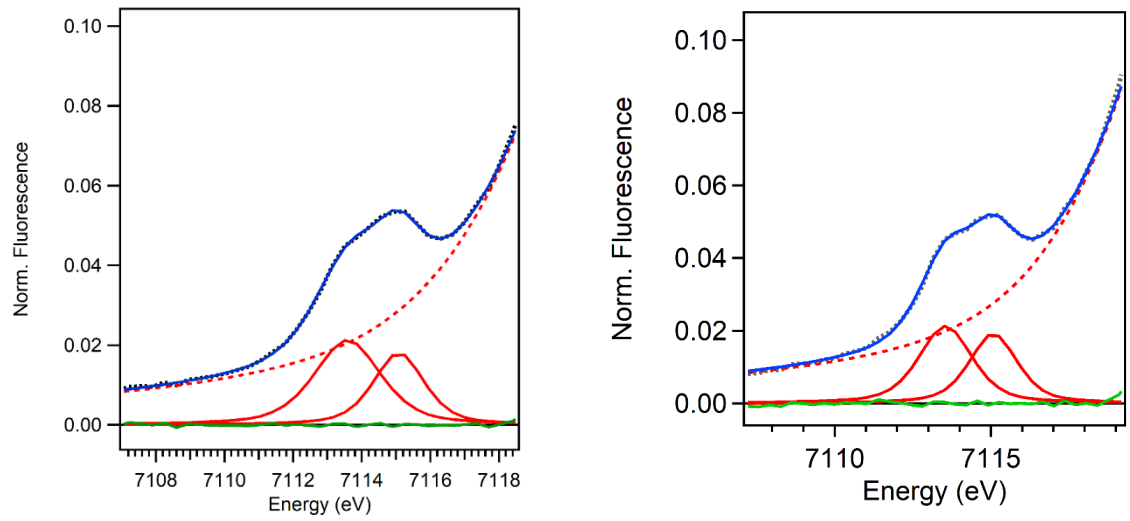

Figure S5. Pre-edge region analysis for **1** (left) and **1**-OAc (right). The experimental data (black dotted), baseline (red dashed), pre-edge peak components (red solid), residuals (green solid), and total fit (blue solid) are shown. Pre-edge area: 8.1 units for **1** and 7.8 units for **1**-OAc.

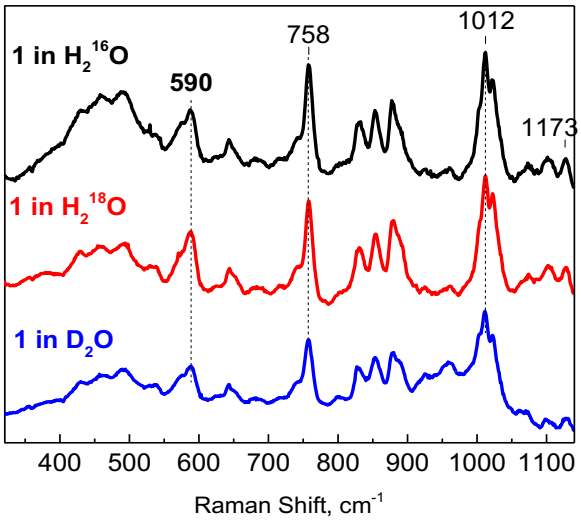

Figure S6: Low-frequency region of the room-temperature Raman spectra of **1** with λ_{exc} = 407 nm incubated in unlabeled water (black trace), $^{18}OH_2$ (red trace), and deuterated water (blue trace). Proteins with diferric μ-oxo bridge chromophores are expected to show a strongly resonance-enhanced $_s$(Fe-O-Fe) between 400 and 500 cm^{-1} that downshifts ~ 20 cm^{-1} with ^{18}O-exchange of the bridging atom.

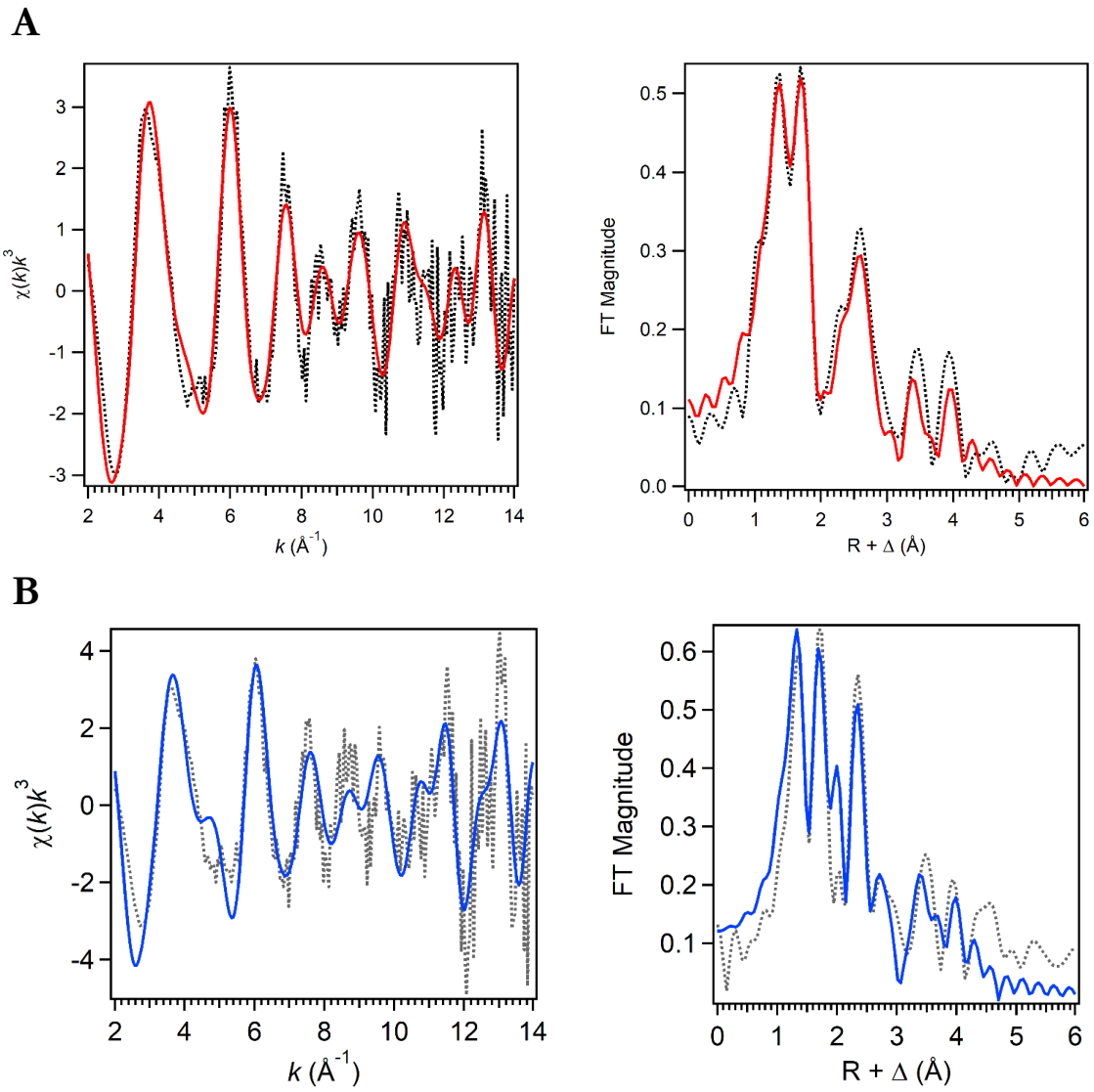

Figure S7. (**A**) Fit (red solid line) of the unfiltered (black dotted) EXAFS data (left) and corresponding Fourier transform (right) of **1** (Table S1, Fit 21). (**B**) Fit (blue solid line) of the unfiltered (black dotted) EXAFS data (left) and corresponding Fourier transform (right) of **1**-OAc (Table S8, Fit 21). Data was fit between k = 2–14 Å^{-1}.

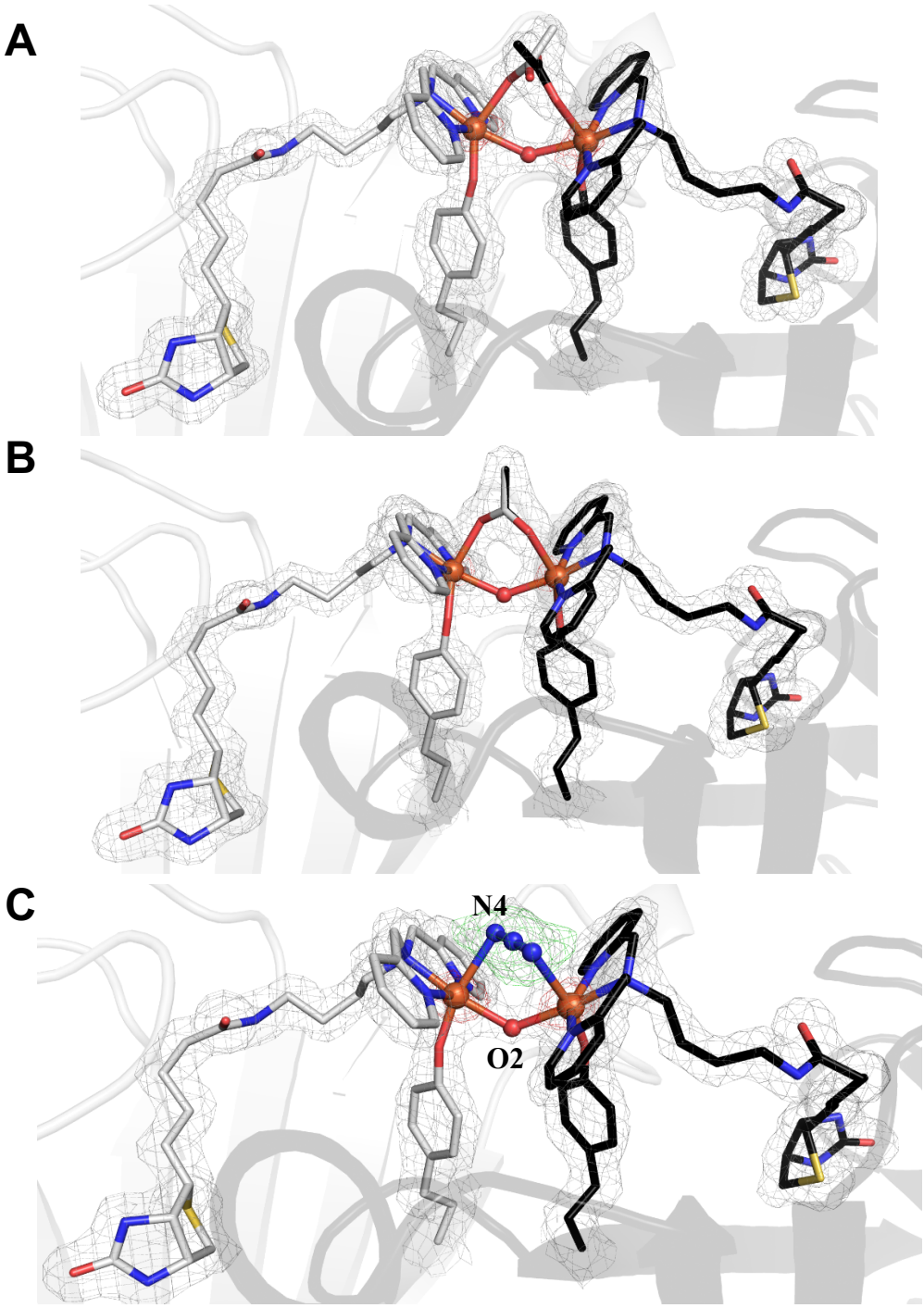

Figure S8. Close-up views of the Fe sites in the molecular structure of **1** (**A**), **1–OAc** (**B**), and **1–N_3** (**C**). For clarity, only one Sav dimer is displayed. The protein is displayed in cartoon representation, and the Fe complex and residues 124 are displayed as sticks. The position of the ligand molecules is indicated by the $2F_o$-F_c electron density (grey, contoured at 1 σ) and anomalous difference density (red, contoured at 4 σ; for C, contoured at 3 σ). Fe is colored in orange, N atoms are in blue, and O atoms/water molecules are in red. The number schemes in **A**, **B,** and **C** are the same as those in Figure 3.

Dimer A

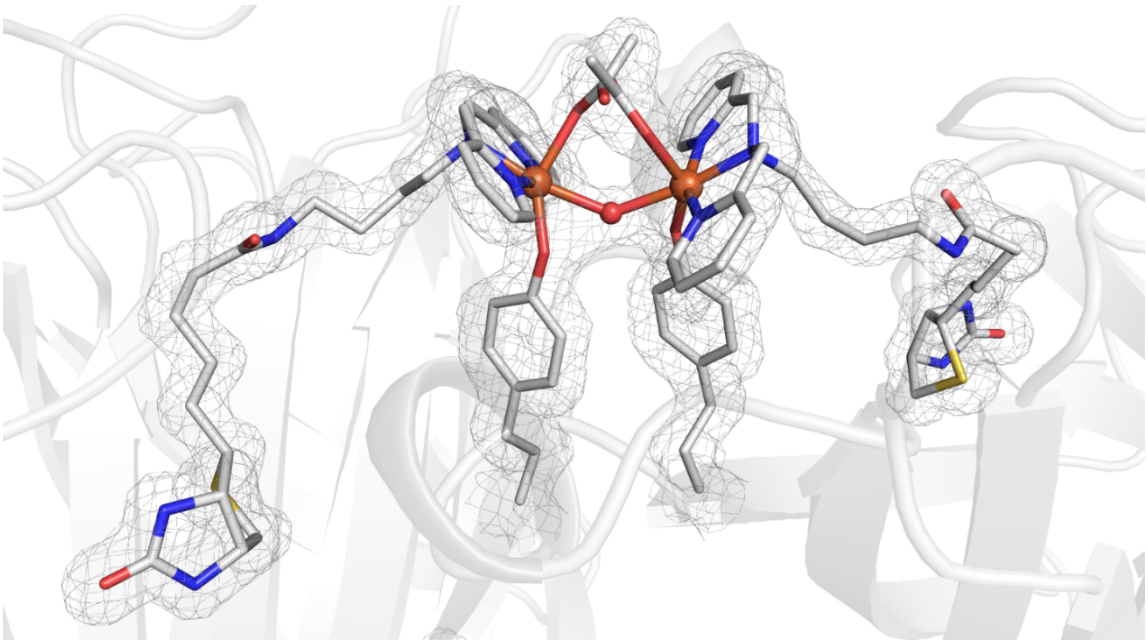

Dimer B

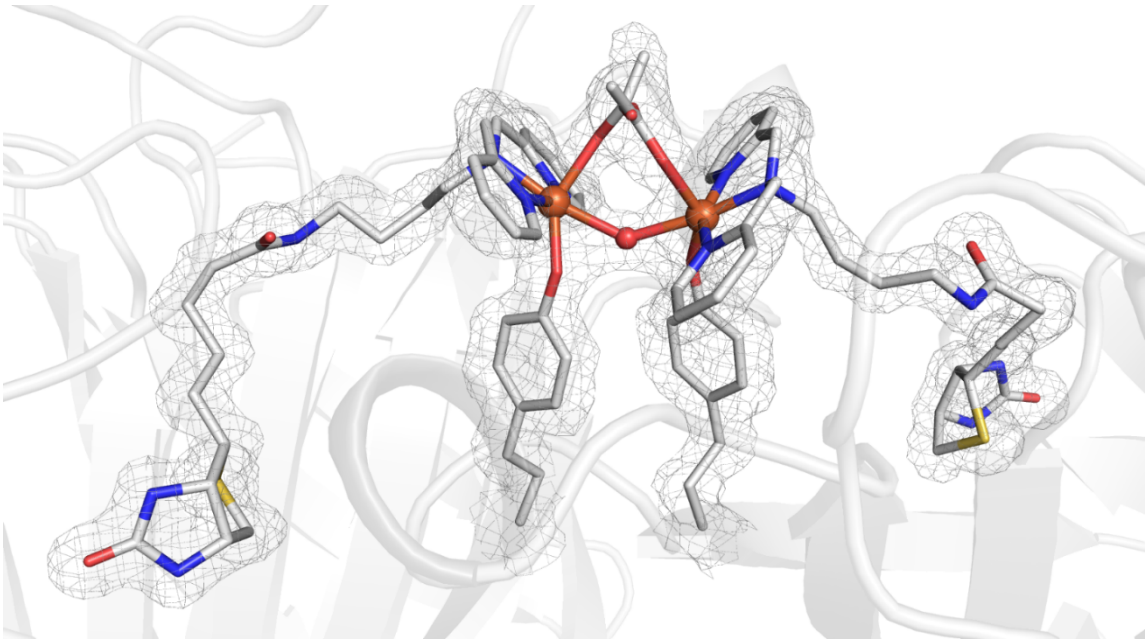

Figure S9. Close-up views of the Fe sites in the molecular structure of **1** solved in C121 symmetry. **Dimers A** and **B** of the tetrameric Sav are shown for clarity. The protein is displayed in cartoon representation, and the Fe complex and residues 124 are displayed as sticks. The position of the ligand molecules is indicated by the $2F_o$-F_c electron density (grey, contoured at 1 σ). Fe is colored in orange, N atoms are in blue, and O atoms/water molecules are in red. The number schemes in **Dimer A** and **Dimer B** are the same as those in Figure 3.

Dimer A

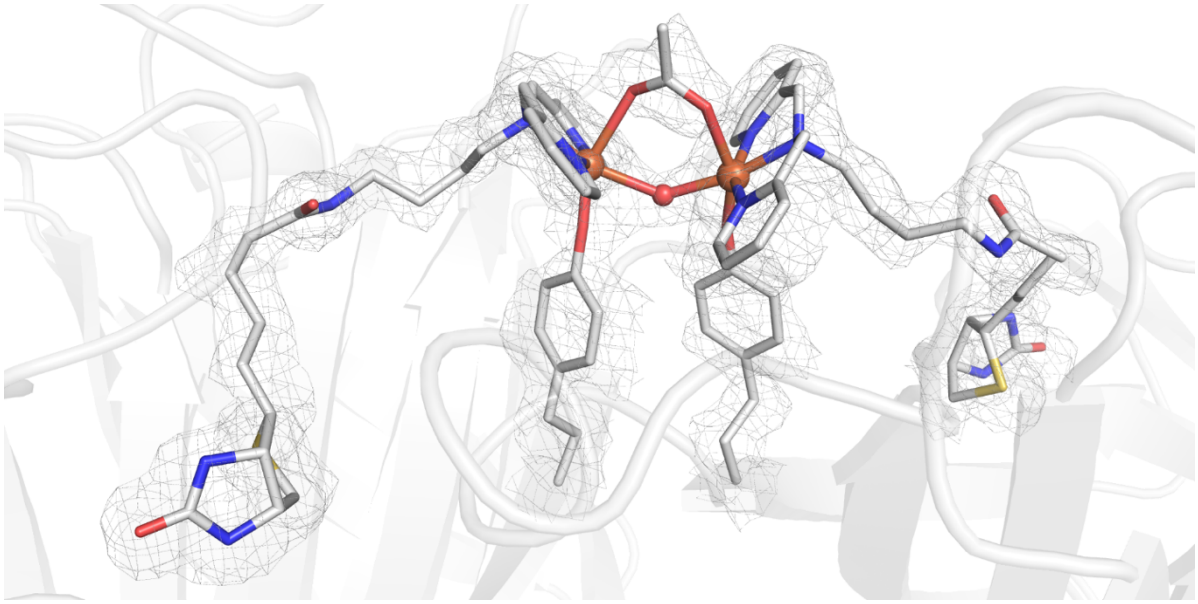

Dimer B

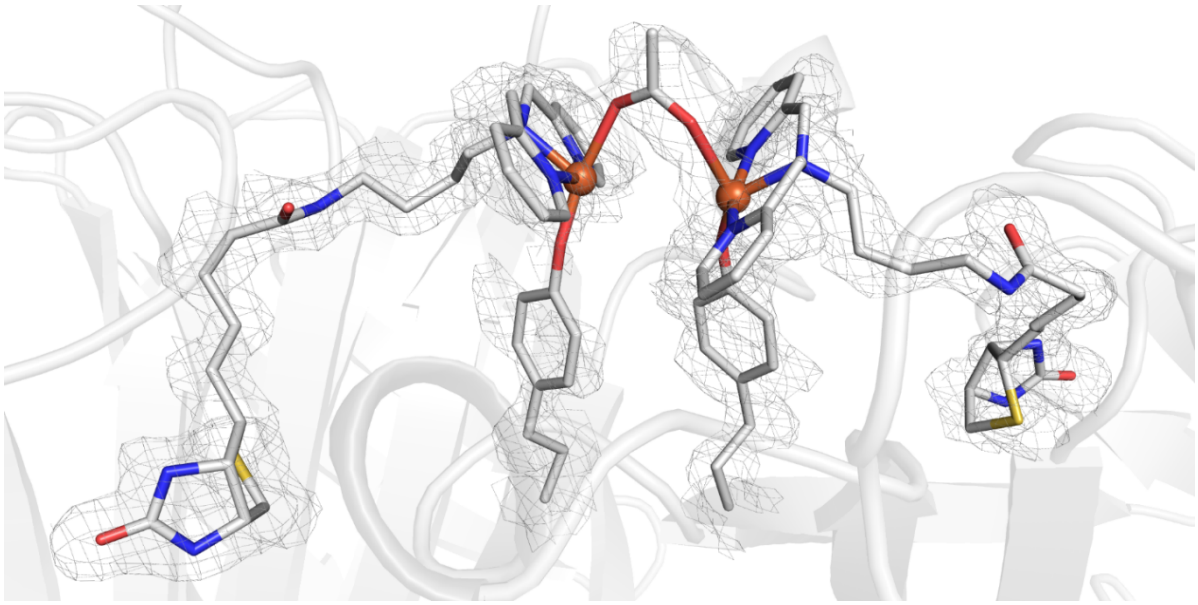

Figure S10. Close-up views of the Fe sites in the molecular structure of **1–OAc** solved in C121 symmetry. **Dimers A** and **B** of the tetrameric Sav are shown for clarity. The protein is displayed in cartoon representation, and the Fe complex and residues 124 are displayed as sticks. The position of the ligand molecules is indicated by the $2F_o$-F_c electron density (grey, contoured at 1 σ). Fe is colored in orange, N atoms are in blue, and O atoms/water molecules are in red. The number schemes in **Dimer A** and **Dimer B** are the same as those in Figure 3.

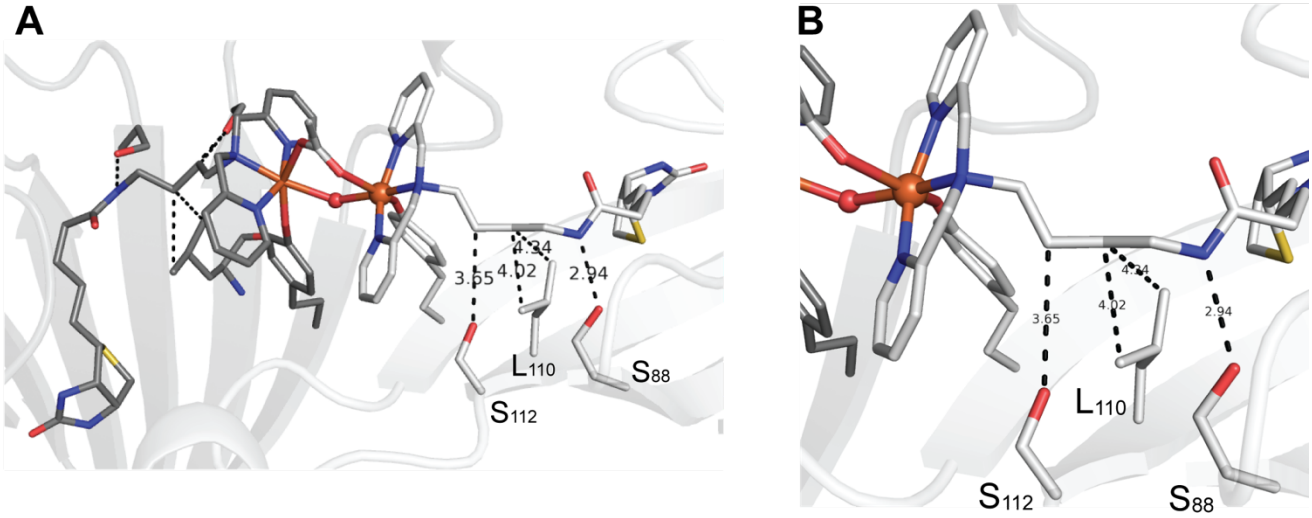

Figure 11. Structure of the dimer highlighting the interactions between side chains of the Sav host and the butyl linkers of the artificial metallocofactor with a full view of the dimer (**A**) and a zoomed in view of one subunit (**B**).

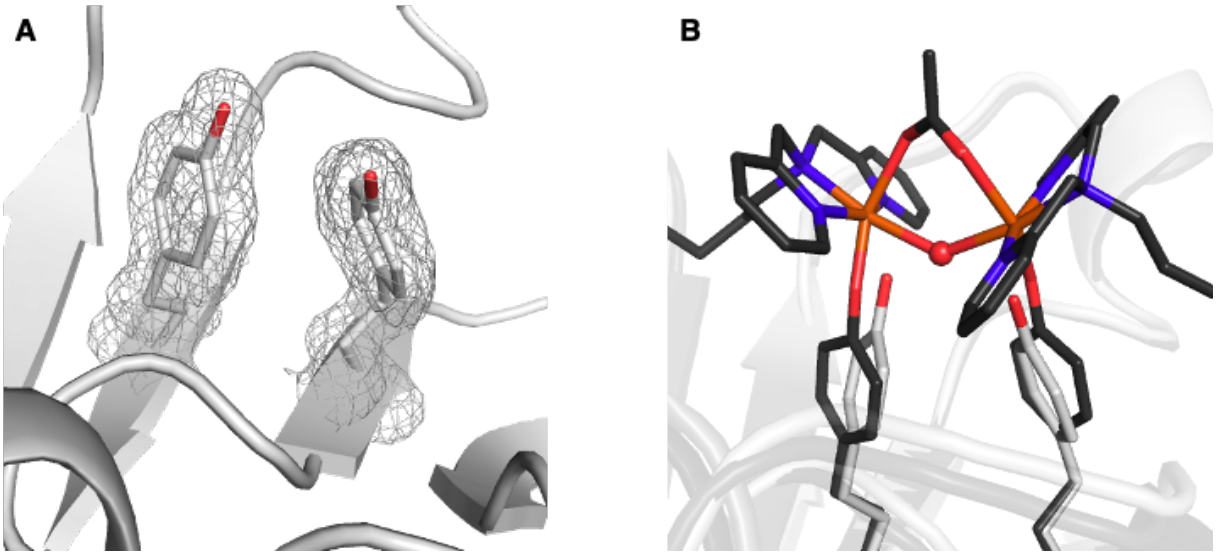

Figure S12. Structure of apo-K_{121}A-L_{124}Y-Sav from XRD measurements showing the position of Y_{124} (**A**) and an overlay of apo-K_{121}A-L_{124}Y-Sav (white) with **1**-OAc (black) (**B**). The position of the side chains at Y_{124} are indicated by the $2F_o$-F_c electron density (grey, contoured at 1 σ).

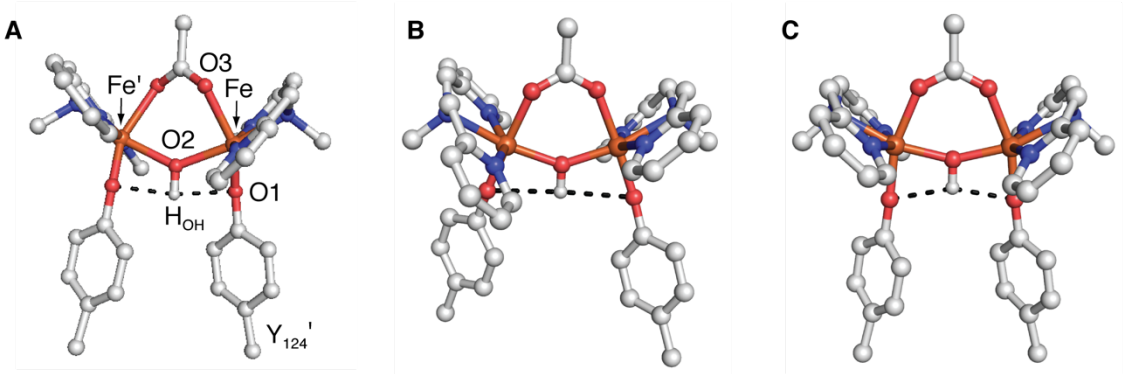

Figure S13. DFT optimized structure of **1**-OAc using XRD coordinates with an unconstrained hydrogen atom placed onto the bridging ligand that shows H-bonds (dashed lines) (**A**, same as Figure 5E), unconstrained DFT optimized structure of the [(dpa)Fe^{III}-(μ-OH)(μ-1,3-carboxylato)-Fe^{III}(dpa)] species (**B**, from DFT-1 from Table 2), and DFT optimized structure of [(dpa)Fe^{III}-(μ-OH)(μ-1,3-carboxylato)-Fe^{III}(dpa)] species with Y_{124} residues frozen at XRD position and the irons to the XRD distance (**C**, form DFT-2 from Table 2). The labelling of the atoms in **B** and **C** are the same as in **A**.

Dimer A

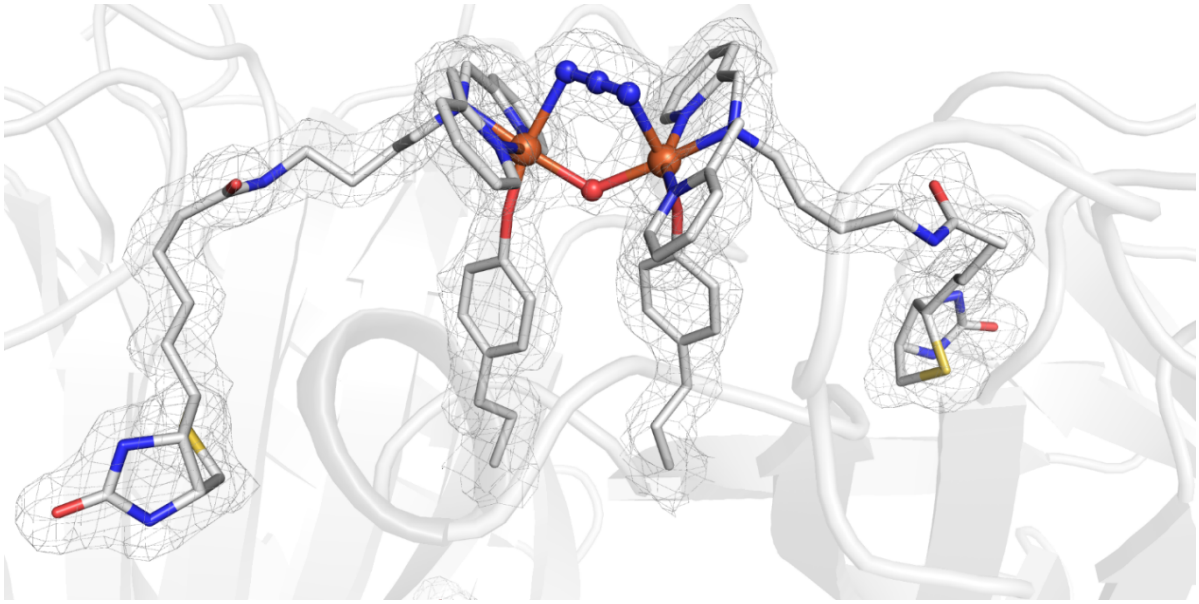

Dimer B

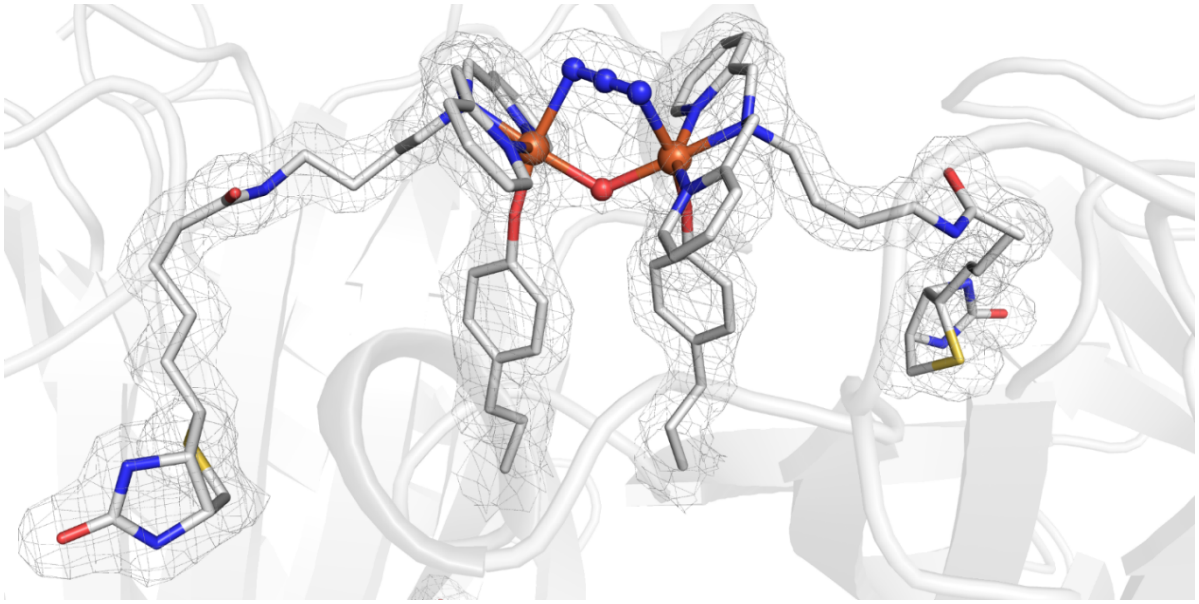

Figure S14. Close-up views of the Fe sites in the molecular structure of **1–N_3** solved in C121 symmetry. **Dimers A** and **B** of the tetrameric Sav are shown for clarity. The protein is displayed in cartoon representation, and the Fe complex and residues 124 are displayed as sticks. The position of the ligand molecules is indicated by the $2F_o$-F_c electron density (grey, contoured at 1 σ). Fe is colored in orange, N atoms are in blue, and O atoms/water molecules are in red. The number schemes in **Dimer A** and **Dimer B** are the same as those in Figure 3.

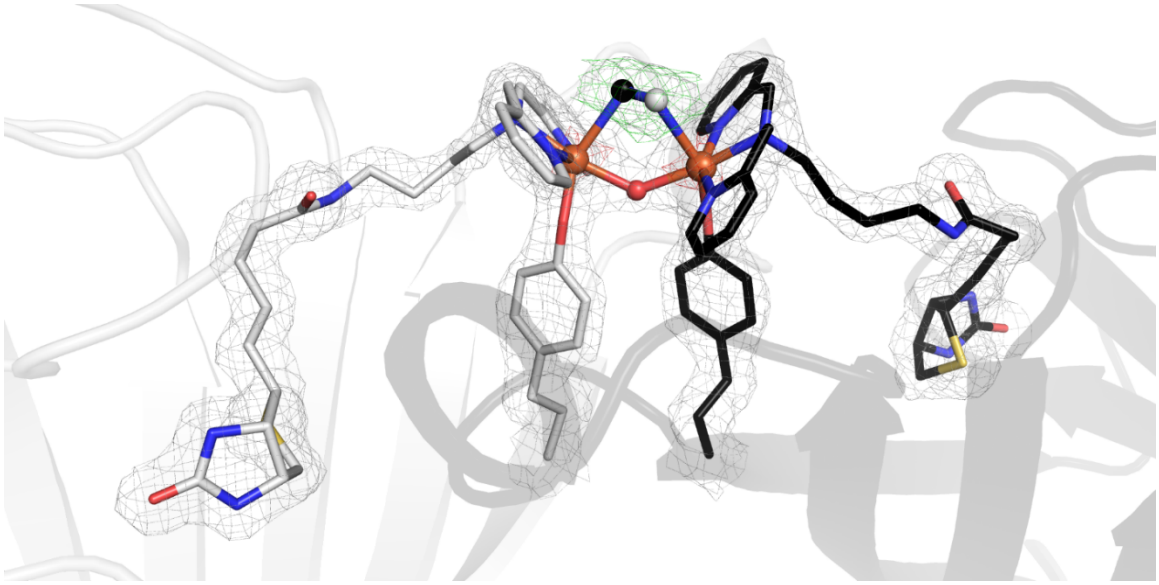

Figure S15. Close-up views of the Fe sites in the molecular structures of **1**–CN. For clarity, only one Sav dimer is displayed. The protein is displayed in cartoon representation, and the Fe complex and residues 124 are displayed as sticks. The position of the ligand molecules is indicated by the $2F_o$-F_c electron density (grey, contoured at 1 σ) and anomalous difference density (red, contoured at 4 σ; for C, contoured at 3 σ). Fe is colored in orange, N atoms are in blue, S atoms are in yellow, and O atoms/water molecules are in red. The number schemes are the same as those in Figure 3.

Dimer A

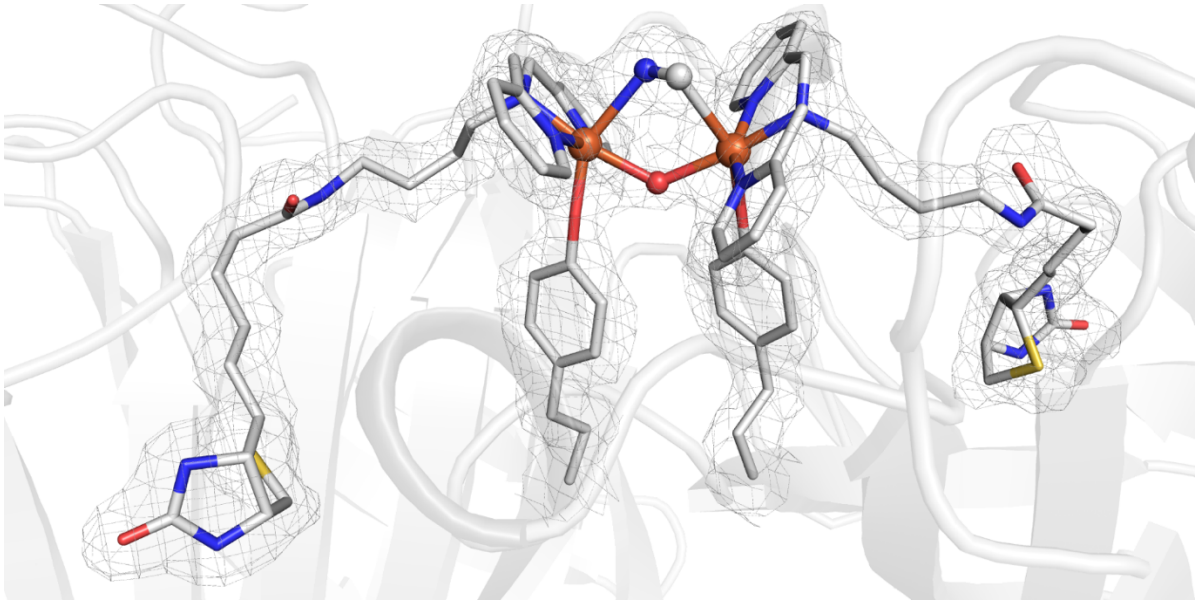

Dimer B

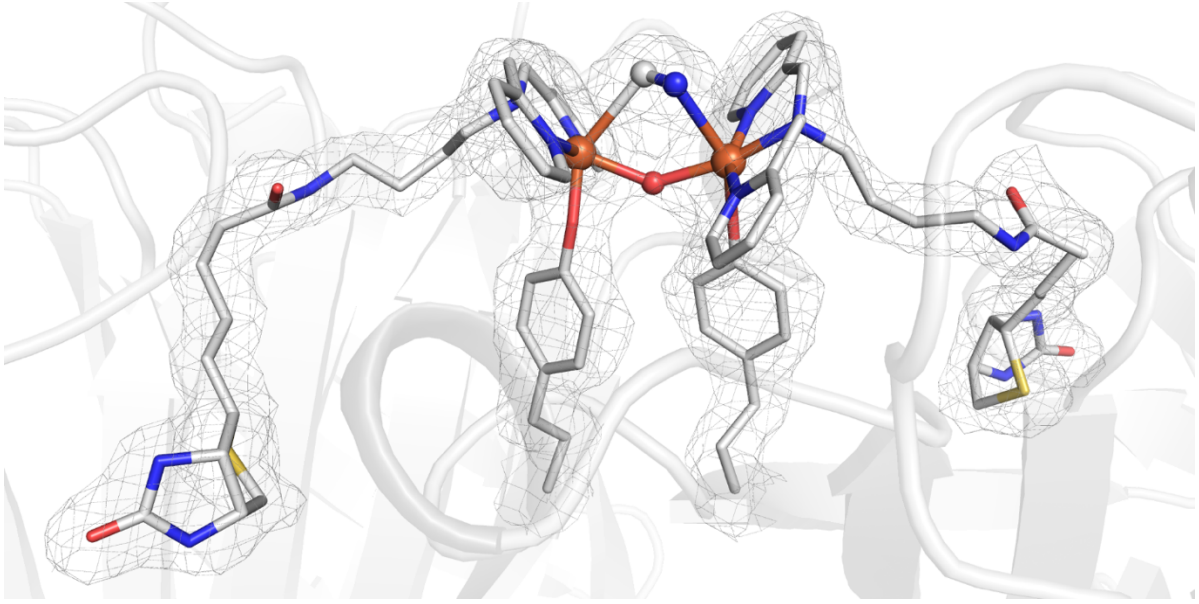

Figure S16. Close-up views of the Fe sites in the molecular structure of **1**–CN solved in C121 symmetry. **Dimers A** and **B** of the tetrameric Sav are shown for clarity. The protein is displayed in cartoon representation, and the Fe complex and residues 124 are displayed as sticks. The position of the ligand molecules is indicated by the $2F_o$-F_c electron density (grey, contoured at 1 σ). Fe is colored in orange, N atoms are in blue, and O atoms/water molecules are in red. The number schemes in **Dimer A** and **Dimer B** are the same as those in Figure 3.

Table S1. Summary of EXAFS best fits for **1** and **1**-OAc**.**

	Fe–N/O			Fe–O/N			Fe···C			Fe···Fe		
Species	**N**	**R(Å)**	**$\sigma^2(10^{-3})$**	**N**	**R(Å)**	**$\sigma^2(10^{-3})$**	**N**	**R(Å)**	**$\sigma^2(10^{-3})$**	**N**	**R(Å)**	**$\sigma^2(10^{-3})$**
1	4	2.10	8.36	1	1.89	5.41	3	3.05	3.57	1	4.02	3.75
							5	4.20	1.61			
1-OAc	4	2.08	6.55	1	1.86	1.62	4	2.94	2.13	1	4.00	0.97
							4	3.10	1.22			
							7	4.18	1.51			

Table S2. EXAFS fit parameters for **1**. Fit 21 corresponds to the most reasonable fit of the data between k = 2 and 14 Å^{-1}.

	Fe–N/O			Fe–O/N			Fe···C			Fe···Fe			GOF		
Fit	**N**	**R(Å)**	**σ^2 (10^{-3})**	**N**	**R(Å)**	**σ^2 (10^{-3})**	**N**	**R(Å)**	**σ^2 (10^{-3})**	**N**	**R(Å)**	**σ^2 (10^{-3})**	**ΔE_0**	**F**	**F'**
1	1	2.13	1.87										8.95	307	782
2	2	2.12	5.71										8.04	236	686
3	3	2.11	9.46										7.03	204	637
4	4	2.09	13.27										5.86	192	617
5	1	2.14	0.89	1	2.01	5.56							4.67	232	680
6	1	2.12	1.88	2	2.02	9.11							5.54	194	621
7	2	2.09	4.21	1	1.94	3.31							6.33	190	615
8	3	2.07	7.84	1	1.90	3.11							5.09	177	594
9	4	2.10	8.03	1	1.89	4.79							3.54	159	562
10	5	2.09	10.43	1	1.87	4.70							3.03	163	569
11	2	2.17	4.25	2	2.02	3.57							4.23	164	571
				1	1.87	2.14									
12	2	2.16	4.45	1	2.04	1.49	3	3.05	3.69				5.79	104	454
				1	1.91	3.07									
13	3	2.12	5.96	1	1.92	5.74	3	3.05	3.44				5.38	109	466
14	3	2.12	5.92	1	1.92	5.61	3	3.05	3.44	1	4.12	13.22	5.14	102	451
15	4	2.11	8.29	1	1.89	5.29	3	3.05	3.53				4.73	107	461
16	4	2.11	8.29	1	1.89	5.32	3	3.05	3.52	1	4.11	12.94	4.75	100	446
17	3	2.12	6.01	1	1.92	5.84	3	3.05	3.55	1	4.07	7.83	5.30	90	422
							1	4.23	-3.20						
18	3	2.12	6.03	1	1.93	5.91	3	3.05	3.58				5.50	103	452
							1	4.23	-1.90						
19	3	2.12	6.02	1	1.92	5.90	3	3.05	3.48				5.48	105	457
							3	4.03	1.61						
							4	4.21	2.00						
20	3	2.12	6.06	1	1.93	5.94	3	3.05	3.47	1	4.03	3.90	5.49	87	417
							5	4.20	1.64						
21	**4**	**2.10**	**8.36**	**1**	**1.89**	**5.41**	**3**	**3.05**	**3.57**	**1**	**4.02**	**3.75**	**4.72**	**84**	**407**
							5	**4.20**	**1.61**						

Table S3. Selected bond lengths (Å) and angles (°) for **1**, **1**–OAc, **1**–N_3, and **1**–CN from XRD measurements

Bond lengths and angles	**1**	**1**–OAc	**1**–N_3	**1**–CN
Fe–O1	1.78	1.82	1.81	1.83
Fe–O2	2.16	2.12	2.14	2.04
Fe–O3	2.17	2.20	–	–
Fe–N1	2.03	2.06	2.10	2.08
Fe–N2	1.98	1.99	2.02	2.01
Fe–N3	1.91	1.92	1.97	1.94
Fe–N4	–	–	2.45	–
Fe–C/N	–	–	–	2.47
O1–Fe–N2	87	82	86	85
O1–Fe–N1	127	121	110	116
O1–Fe–N3	110	112	105	108
O2–Fe–N2	110	105	109	109
O3–Fe–O1	146	151	–	–
O3–Fe–O2	82	86	–	–
O3–Fe–N1	87	84	–	–
O3–Fe–N2	99	91	–	–
O3–Fe–N3	78	86	–	–
O1–Fe–N4	–	–	165	–
O1–Fe–O2	65	70	78	74
N1–Fe–N2	77	77	75	76
N1–Fe–N3	76	78	77	76
N1–Fe–N4	–	–	85	–
N1–Fe–O2	168	170	172	169
N2–Fe–N3	153	155	152	152
N2–Fe–N4	–	–	96	–
N3–Fe–N4	–	–	80	–
N3–Fe–O2	97	100	99	99
N4–Fe–O2	–	–	88	–
Fe–O2–Fe’	133	134	126	132
Fe···Fe’	3.96	3.91	3.82	3.73
Fe–N4–N5	–	–	96	–
O1–Fe–C/N	–	–	–	149
O2–Fe–C/N	–	–	–	80
N1–Fe–C/N	–	–	–	91
N2–Fe–C/N	–	–	–	87
N3–Fe–C/N	–	–	–	93
Fe–C/N–C/N	–	–	–	109

Table S4. X-ray Crystallography Data Processing and Refinement Statistics for $I4_122$ symmetry solutions of **1**, **1**–OAc, and **1**–N_3.

Identification			
Sav Mutant Fe complex	$K_{121}A$-$L_{124}Y$ $[Fe_2^{III}$(biot-bu-dpa)$_2$(OAc)(μ–O)$(O_{Y124})_2]$ (**1**)	$K_{121}A$-$L_{124}Y$ $[Fe_2^{III}$(biot-bu-dpa)$_2$(μ–1,3–OAc)(μ–O)$(O_{Y124})_2]$ (**1**–OAc)	$K_{121}A$-$L_{124}Y$ $[Fe_2^{III}$(biot-bu-dpa)$_2$(μ–1,3–N_3)(μ–O)$(O_{Y124})_2]$ (**1**–N_3)
PDB Code	6VOZ	6VO9	6VOB
Fe complex PDB 3-letter code	KM3	KM3	KM3
Data Processing			
Unit Cell	a, b, c = 57.7 Å, 57.7 Å, 184.2 Å α, β, γ = 90°	a, b, c = 57.9 Å, 57.9 Å, 184.7 Å α, β, γ = 90°	a, b, c = 57.7 Å, 57.7 Å, 183.8 Å α, β, γ = 90°
Space Group	$I4_122$	$I4_122$	$I4_122$
Resolution (Å)	37.29 – 1.30	46.16 – 1.50	55.02 – 1.70
Highest resolution shell (Å)	1.32 – 1.30	1.53 – 1.50	1.73 – 1.70
R_{merge} (%)	7.1 (145)	8.2 (71)	17 (193)
No. of unique reflections	38785 (1888)	21730 (953)	17637 (897)
Multiplicity	13.3 (12.6)	6.4 (5.4)	25.4 (24.5)
I/Sig(I)	19.2 (1.5)	11.6 (1.9)	17.0 (2.6)
Completeness	99.9 (99.2)	84.5 (75.3)	100 (100)
CC(1/2)	0.999 (0.79)	0.993 (0.81)	0.998 (0.772)
Beamline	SSRL 12.2	SSRL 12.2	ALS 8.2.1
Structure Refinement			
R_{work}	0.18	0.18	0.17
R_{free}	0.21	0.21	0.20
Rmsd bond length (Å)	0.018	0.014	0.016
Rmsd bond angle (°)	2.841	2.865	2.712
Rmsd compared to biotin-Sav WT (PDB 1STP) (Å)	0.64	0.65	0.63
No. ligands			
Fe complex	1	1	1
Water	119	93	95
Acetate	1	1	1

Table S5. Summary of structural details for $I4_122$ symmetry solutions of **1**, **1**–OAc, and **1**–N_3.

PDB Code	6VOZ	6VO9	6VOB
Complex	**1**	**1**–OAc	**1**–N_3
Electron density at Fe in F_o–F_c omit map (σ)	19	25	25
Anomalous dispersion density at Fe (σ)	10	5	9
Geometry of Fe complex	Distorted octahedral	Distorted octahedral	Distorted octahedral
Coordination number of Fe complex	6	6	6
Occupancy of Fe complex (%)	60	100	100
B-factor (Å^2)			
Overall protein	19	17	17
L124Y	20	20	22
K121A	15	14	14
Fe complex	28	22	22
DPA	28	22	21
Fe	28	30	30
Acetate	24	27	–
Azide	–	–	25
Distance Fe −Fe (Å)	3.96	3.91	3.82

Table S6. X-ray Crystallography Data Processing and Refinement Statistics for C121 symmetry solutions of **1**, **1**–OAc, and **1**–N_3.

Identification			
Sav Mutant	$K_{121}A$-$L_{124}Y$	$K_{121}A$-$L_{124}Y$	$K_{121}A$-$L_{124}Y$
Fe complex	$[Fe_2^{III}$(biot-bu-dpa)$_2$(OAc)(μ–O)$(O_{Y124})_2]$ (**1**)	$[Fe_2^{III}$(biot-bu-dpa)$_2$(μ–1,3–OAc)(μ–O)$(O_{Y124})_2]$ (**1**–OAc)	$[Fe_2^{III}$(biot-bu-dpa)$_2$(μ–1,3–N_3)(μ–O)$(O_{Y124})_2]$ (**1**–N_3)
PDB Code	6VP1	6VP3	6VP2
Fe complex PDB 3-letter code	KM3	KM3	KM3
Data Processing			
Unit Cell	a, b, c = 193.0 Å, 57.7 Å, 57.7 Å α, β, γ = 90°, 107.4°, 90°	a, b, c = 193.5 Å, 57.9 Å, 57.9 Å α, β, γ = 90°, 107.4°, 90°	a, b, c = 192.8 Å, 57.6 Å, 57.7 Å α, β, γ = 90°, 107.4°, 90°
Space Group	C121	C121	C121
Resolution (Å)	37.29 – 1.45	46.16 – 1.65	55.00 – 1.80
Highest resolution shell (Å)	1.47 – 1.45	1.68 – 1.65	1.84 – 1.80
R_{merge} (%)	5.4 (66)	7.4 (28)	14 (92)
No. of unique reflections	104561 (5170)	47899 (2078)	55911 (3174)
Multiplicity	3.6 (3.3)	2.4 (2.3)	6.8 (6.4)
I/Sig(I)	13.0 (2.4)	7.7 (2.3)	10.2 (2.4)
Completeness	97.6 (97.2)	65.2 (57.7)	99.6 (98)
CC(1/2)	0.989 (0.795)	0.989 (0.905)	0.995 (0.765)
Beamline	SSRL 12.2	SSRL 12.2	ALS 8.2.1
Structure Refinement			
R_{work}	0.18	0.18	0.17
R_{free}	0.20	0.22	0.20
Rmsd bond length (Å)	0.016	0.013	0.013
Rmsd bond angle (°)	3.022	2.868	2.679
Rmsd compared to biotin-Sav WT (PDB 1STP) (Å)	0.63	0.64	0.63
No. ligands			
Fe complex	4	4	4
Water	214	498	424
Acetate	2	2	–
Azide	–	–	2

Table S7. Summary of structural details for C121 symmetry solutions of **1**, **1**–OAc, and **1**–N_3.

PDB Code	6VP1	6VP3	6VP2
Complex	**1**	**1**–OAc	**1**–N_3
Electron density at Fe in F_o–F_c omit map (σ)	19	20	25
Anomalous dispersion density at Fe (σ)	–	–	–
Geometry of Fe complex	Distorted octahedral	Distorted octahedral	Distorted octahedral
Coordination number of Fe complex	6	6	6
Occupancy of Fe complex (%)	80	100	100
***B-factor (Å^2)**			
Overall protein	18	16	17
L124Y	20	20	23
K121A	15	14	14
Fe complex	29	22	22
DPA	28	22	21
Fe	34	28	31
Acetate	27	28	–
Azide	–	–	23
Dimer A Distance Fe–Fe (Å)	4.01	3.95	3.75
Dimer B Distance Fe–Fe (Å)	3.99	4.02	3.71

*B-factors were averaged from the Sav tetramer

Table S8. Bond lengths and distances for **1** from C121 symmetry solution.

Bond lengths (Å) and angles (°)	**Monomer 1**	**Monomer 2**	**Monomer 3**	**Monomer 4**
Fe–O1	1.88	1.90	1.86	1.89
Fe–O2	2.16	2.14	2.16	2.12
Fe–O3	2.22	–	2.15	–
Fe'–O3'		2.18	–	2.13
Fe'–O4	–	3.60	–	3.50
Fe–O4'	3.56	–	3.57	–
Fe–N1	2.03	2.03	2.03	2.03
Fe–N2	1.94	1.95	1.94	1.95
Fe–N3	1.97	1.97	1.97	1.98
	Dimer A (1 & 2)		**Dimer B (3 & 4)**	
Fe–O2–Fe'	138		138	
Fe···Fe'	4.01		3.99	

Table S9. Bond lengths and distances for **1**–OAc from the C121 symmetry solution.

Bond lengths (Å) and angles (°)	**Monomer 1**	**Monomer 2**	**Monomer 3**	**Monomer 4**
Fe–O1	1.78	1.69	1.76	1.81
Fe–O2	2.05	2.26	–	–
Fe–O3	2.22	–	2.18	–
Fe'–O3'	–	2.35	–	2.40
Fe–N1	2.03	2.02	2.05	2.02
Fe–N2	1.98	1.95	1.99	1.97
Fe–N3	1.91	1.93	1.92	1.90
	Dimer A (1 & 2)		**Dimer B (3 & 4)**	
Fe–O2–Fe'	132		–	
Fe···Fe'	3.95		4.02	

Table S10. EXAFS fit parameters for **1**-OAc. Fit 21 corresponds to most reasonable fit of the data between k = 2 – 14 Å^{-1}.

	Fe–N/O			**Fe–O/N**			**Fe···C**			**Fe···Fe**				**GOF**	
Fit	N	R(Å)	$\sigma^2(10^{-3})$	N	R(Å)	$\sigma^2(10^{-3})$	N	R(Å)	$\sigma^2(10^{-3})$	N	R(Å)	$\sigma^2(10^{-3})$	ΔE_0	F	F'
1	1	2.12	-0.50										9.47	516	809
2	2	2.12	3.23										8.57	481	780
3	3	2.11	7.83										7.66	477	777
4	4	2.09	13.39										6.56	473	776
5	2	2.10	1.23	1	1.91	2.86							2.18	406	718
6	3	2.09	3.81	1	1.88	2.05							2.12	386	699
7	4	2.08	6.33	1	1.87	1.79							2.06	383	697
8	5	2.08	8.82	1	1.86	1.80							1.96	395	707
9	4	2.09	6.39	1	1.87	1.91	1	3.01	5.38				2.65	364	679
10	4	2.09	6.43	1	1.87	1.98	2	3.01	6.67				3.05	353	668
11	4	2.09	6.45	1	1.87	1.99	3	3.02	7.98				3.25	347	663
12	4	2.08	6.52	1	1.86	1.64	1	2.92	-4.00				1.88	309	626
							1	3.06	-4.30						
13	4	2.08	6.62	1	1.86	1.78	1	2.90	-3.60				2.52	301	618
							3	3.04	0.75						
14	4	2.08	6.49	1	1.86	1.75	3	2.92	1.03				2.70	327	646
							4	3.08	1.49						
15	4	2.07	4.37	1	1.87	0.56	3	2.93	0.30				3.40	325	642
				1	2.23	4.06	4	3.09	0.72						
16	4	2.11	4.48	1	1.89	2.00	4	3.05	8.93				5.71	327	644
				1	2.30	1.81									
17	4	2.08	6.47	1	1.87	1.88	4	3.01	9.18				2.83	337	652
18	4	2.08	6.55	1	1.86	1.54	4	2.93	2.30	1	3.99	4.87	1.94	332	649
							4	3.09	1.46						
19	4	2.08	6.52	1	1.87	1.91	4	3.02	8.76	1	4.02	1.41	2.91	292	608
							6	4.20	1.09						
20	2	2.08	0.00	2	1.91	4.06	4	2.94	1.71				3.02	323	640
				2	2.17	5.83	4	3.10	0.76						
21	**4**	**2.08**	**6.55**	**1**	**1.86**	**1.62**	**4**	**2.94**	**2.13**	**1**	**4.00**	**0.97**	**2.98**	**276**	**591**
							4	**3.10**	**1.22**						
							7	**4.18**	**1.51**						

Table S11. X-ray Crystallography Data Processing and Refinement Statistics for $I4_122$ symmetry solutions of apo-$K_{121}A$-$L_{124}Y$-Sav.

Identification	
Sav Mutant	$K_{121}A$-$L_{124}Y$
PDB Code	7KNL
Data Processing	
Unit Cell	a, b, c = 57.6 Å, 57.6 Å, 171.9 Å α, β, γ = 90°, 90°, 90°
Space Group	$I4_122$
Resolution (Å)	40.76 – 1.35
Highest resolution shell	1.37 – 1.35
R_{merge} (%)	3.1 (95)
No. of unique reflections	32429 (1593)
Multiplicity	13.7 (13.6)
I/Sig(I)	38.3 (2.8)
Completeness	100 (99.9)
CC(1/2)	1.000 (0.879)
Beamline	ALS 5.0.2
Structure Refinement	
R_{work}	0.22
R_{free}	0.24
Rmsd bond length (Å)	0.015
Rmsd bond angle (°)	2.116
Rmsd compared to Sav WT (PDB 3RY1) (Å)	3.1
No. ligands	
Water	63

Table S12. Summary of structural details for $I4_122$ symmetry solutions of apo-$K_{121}A$-$L_{124}Y$-Sav.

PDB Code	7KNL
B-factor (Å²)[a]	
Overall protein	23
L124Y	21
K121A	31

[a]B-factors were averaged from the Sav monomer

Table S13. DFT calculated geometrical and exchange parameters obtained for the [(dpa)Fe^{III}-(μ-OH_n)(μ-1,3-carboxylato)-Fe^{III}(dpa)] species.[a]

	DFT_O[b]	DFT_{H2O}[c]	DFT-3[d]
Fe···Fe'	3.91	3.91	3.91
Fe–O1	1.82	1.82	1.83
Fe–O2	2.12	2.12	2.06
Fe–O3	2.23	2.23	2.08
O1…H_{O2}	**–**	1.55	2.53
O1–Fe-–O2	70	70	90
Fe–O2–Fe'	134	134	143
J_{DFT} (cm^{-1})	-275	2	22

[a] bond distances and angles reported in Å and deg; geometrical parameters in boldface are affected by optimization, [b] XRD structure with oxo bridge, [c] XRD structure with water bridge; the positions of the bridging water protons have been optimized, [d] For optimization of OH bridged species with the irons, the $C_®$ atoms of the Y_{124} residues and the C atoms of the linkers connected to the tertiary amines frozen to XRD positions.

Table S14. Bond lengths and distances for **1**–N_3 from C121 symmetry solution.

Bond lengths (Å) and angles (°)	**Monomer 1**	**Monomer 2**	**Monomer 3**	**Monomer 4**
Fe–O1	1.77	1.77	1.79	1.78
Fe–O2	2.10	2.14	2.11	2.12
Fe–N4	2.34	–	2.29	–
Fe'–N4'	–	2.33	–	2.30
Fe–N1	2.07	2.08	2.07	2.09
Fe–N2	2.01	2.00	2.02	2.01
Fe–N3	1.95	1.94	1.96	1.95
	Dimer A (1 & 2)		**Dimer B (3 & 4)**	
Fe–O2–Fe'	124		122	
Fe···Fe'	3.75		3.71	

Table S15. X-ray Crystallography Data Processing and Refinement Statistics for $I4_122$ and C121 symmetry solutions of **1–CN**.

Identification		
Sav Mutant	$K_{121}A$-$L_{124}Y$	$K_{121}A$-$L_{124}Y$
Fe complex	$[Fe_2^{III}$(biot-bu-dpa)$_2$(μ–1,2–CN)(μ–O)$(O_{Y124})_2]$ (**1**–CN)	$[Fe_2^{III}$(biot-bu-dpa)$_2$(μ–1,3–CN)(μ–O)$(O_{Y124})_2]$ (**1**–CN)
PDB Code	7KBY	7KBZ
Fe complex PDB 3-letter code	KM3	KM3
Data Processing		
Unit Cell	a, b, c = 57.6 Å, 57.6 Å, 183.5 Å α, β, γ = 90°	a, b, c = 192.3 Å, 57.6 Å, 57.6 Å α, β, γ = 90°, 107.4°, 90°
Space Group	$I4_122$	C121
Resolution (Å)	45.86 – 1.70	45.86 – 1.90
Highest resolution shell (Å)	1.73 – 1.70	1.94 – 1.90
R_{merge} (%)	21 (184)	15 (82)
No. of unique reflections	17537 (899)	45992 (2913)
Multiplicity	11.7 (11.7)	3.3 (3.0)
I/Sig(I)	9.1 (1.8)	6.3 (1.7)
Completeness	100 (100)	97.1 (96.3)
CC(1/2)	0.997 (0.380)	0.990 (0.467)
Beamline	ALS 5.0.2	ALS 5.0.2
Structure Refinement		
R_{work}	0.19	0.19
R_{free}	0.22	0.12
Rmsd bond length (Å)	0.013	0.016
Rmsd bond angle (°)	2.685	2.705
Rmsd compared to biotin-Sav WT (PDB 1STP) (Å)	0.64	0.62
No. ligands		
Fe complex	1	1
Water	71	275
SCN	–	–
CN	1	2

Table S16. Summary of structural details for **1**–CN.

PDB Code	Unpublished	Unpublished
Complex	**1**–CN ($I4_122$)	**1**–CN (C121)
Electron density at Fe in F_o–F_c omit map (σ)	21	17
Anomalous dispersion density at Fe (σ)	5	–
Geometry of Fe complex	Distorted octahedral	Distorted octahedral
Coordination number of Fe complex	6	6
Occupancy of Fe complex (%)	100	100
***B-factor (Å^2)**		
Overall protein	21	22
L124Y	27	30
K121A	18	21
Fe complex	34	36
DPA	33	35
Fe	46	55
Isothiocyanate	–	–
Cyanide		24
Fe–Fe (Å)	3.73	
Dimer A Distance Fe–Fe (Å)	–	3.83
Dimer B Distance Fe–Fe (Å)	–	3.82

*B-factors were averaged from the Sav tetramer

Table S17. Bond lengths and distances for **1**–CN from C121 symmetry solution.

Bond lengths (Å) and angles (°)	**Monomer 1**	**Monomer 2**	**Monomer 3**	**Monomer 4**
Fe–O1	1.81	1.81	1.77	1.82
Fe–O2	2.12	2.16	2.05	2.04
Fe–C/N	2.47	–	2.60	–
Fe'–C/N'	–	2.48	–	2.53
Fe–N1	2.06	2.06	2.05	2.05
Fe–N2	2.01	2.00	2.00	2.00
Fe–N3	1.94	1.93	1.94	1.94
	Dimer A (1 & 2)		**Dimer B (3 & 4)**	
Fe–O2–Fe'	127		139	
Fe···Fe'	3.83		3.82	

Table S18. Vibrational Data for Related Di-Fe Species with Azide Ions.[16]

	ν(Fe-N_3)	$\Delta^{15}NN_2$	$\Delta^{15}N_2$	ν_{as}(NNN)	$\Delta^{15}NN_2$	$\Delta^{15}N_2$	references
			μ-1,3 bridging azide				
1-N_3	396	-3	-9	2088/2060	-13	-71	This work
Δ9D-azide at pH 6.2	380	-4		2100	-11		15
			μ1-terminal azide				
Hemerythrin-azide	375			2048	-6/-17		16
Δ9D-azide at pH 7.8	378	-4		2073	-2/-14		15
MMOH-azide	370	-3		2077	-4/-18		17

References

(1) Pangborn, A. B.; Giardello, M. A.; Grubbs, R. H.; Rosen, R. K.; Timmers, F. J. Safe and Convenient Procedure for Solvent Purification. *Organometallics* **1996**, *15*, 1518–1520.

(2) Chambers, J. M.; Lindqvist, L. M.; Webb, A.; Huang, D. C. S.; Savage, G. P.; Rizzacasa, M. A. Synthesis of Biotinylated Episilvestrol : Highly Selective Targeting of the Translation Factors EIF4AI / II. *Org. Lett.* **2013**, *15*, 1406–1409.

(3) Incarvito, C.; Lam, M.; Rhatigan, B.; Rheingold, A. L.; Qin, C. J.; Gavrilova, A. L.; Bosnich, B. Bimetallic Reactivity. Preparations, Properties and Structures of Complexes Formed by Unsymmetrical Binucleating Ligands Bearing 4- and 6-Coordinate Sites Supported by Alkoxide Bridges. *Dalton Trans.* **2001**, *23*, 3478–3488.

(4) Miller, K. R.; Paretsky, J. D.; Follmer, A. H.; Heinisch, T.; Mittra, K.; Gul, S.; Kim, I. S.; Fuller, F. D.; Batyuk, A.; Sutherlin, K. D.; Brewster, A. S.; Bhowmick, A.; Sauter, N. K.; Kern, J.; Yano, J.; Green, M. T.; Ward, T. R.; Borovik, A. S. Artificial Iron Proteins: Modeling the Active Sites in Non-Heme Dioxygenases. *Inorg. Chem.* **2020**, *59*, 6000–6009.

(5) Petasis, D. T.; Hendrich, M. P. Quantitative Interpretation of Multifrequency Multimode EPR Spectra of Metal Containing Proteins, Enzymes, and Biomimetic Complexes. *Methods Enzym.* **2015**, *563*, 171–208.

(6) Matsumura, H.; Hayashi, T.; Chakraborty, S.; Lu, Y.; Moënne-Loccoz, P. The Production of Nitrous Oxide by the Heme/Nonheme Diiron Center of Engineered Myoglobins (FeBMbs) Proceeds through a Trans -Iron-Nitrosyl Dimer. *J. Am. Chem. Soc.* **2014**, *136*, 2420–2431.

(7) Hayashi, T.; Caranto, J. D.; Matsumura, H.; Kurtz, D. M.; Moënne-Loccoz, P. Vibrational Analysis of Mononitrosyl Complexes in Hemerythrin and Flavodiiron Proteins: Relevance to Detoxifying No Reductase. *J. Am. Chem. Soc.* **2012**, *134*, 6878–6884.

(8) Lu, S.; Sazinsky, M. H.; Whittaker, J. W.; Lippard, S. J.; Moënne-Loccoz, P. Fourier Transform Infrared Characterization of the Azido Complex of Methane Monooxygenase Hydroxylase from Methylococcus Capsulatus (Bath). *J. Am. Chem. Soc.* **2005**, *127*, 4148–4149.

(9) George, G. N. In EXAFSPAK: A Suite of Computer Programs for Analysis of X-Ray Absorption Spectra. **1990**.

(10) Ankudinov, A.; Ravel, B. Real-Space Multiple-Scattering Calculation and Interpretation of x-Ray-Absorption near-Edge Structure. *Phys. Rev. B - Condens. Matter Mater. Phys.* **1998**, *58*, 7565–7576.

(11) Wojdyr, M. A General-Purpose Peak Fitting Program. *J. Appl. Crystallogr* **2010**, *43*, 1126–1128.

(12) Mallin, H.; Hestericová, M.; Reuter, R.; Ward, T. R. Library Design and Screening Protocol for Artificial Metalloenzymes Based on the Biotin-Streptavidin Technology. *Nat. Protoc.* **2016**, *11*, 835–852.
(13) Kabsch, W. XDS. *Acta Crystallogr. Sect. D Biol. Crystallogr.* **2010**, *66*, 125–132.
(14) Emsley, P.; Cowtan, K. Coot: Model-Building Tools for Molecular Graphics. *Acta Crystallogr. Sect. D Biol. Crystallogr.* **2004**, *60*, 2126–2132.
(15) Gaussian 09, Revision D.01, M. J. Frisch, G. W. Trucks, H. B. Schlegel, G. E. Scuseria, M. A. Robb, J. R. Cheeseman, G. Scalmani, V. Barone, B. Mennucci, G. A. Petersson, H. Nakatsuji, M. Caricato, X. Li, H. P. Hratchian, A. F. Izmaylov, J. Bloino, G. Zheng, J. L. Sonnenberg, M. Hada, M. Ehara, K. Toyota, R. Fukuda, J. Hasegawa, M. Ishida, T. Nakajima, Y. Honda, O. Kitao, H. Nakai, T. Vreven, J. A. Montgomery, Jr., J. E. Peralta, F. Ogliaro, M. Bearpark, J. J. Heyd, E. Brothers, K. N. Kudin, V. N. Staroverov, T. Keith, R. Kobayashi, J. Normand, K. Raghavachari, A. Rendell, J. C. Burant, S. S. Iyengar, J. Tomasi, M. Cossi, N. Rega, J. M. Millam, M. Klene, J. E. Knox, J. B. Cross, V. Bakken, C. Adamo, J. Jaramillo, R. Gomperts, R. E. Stratmann, O. Yazyev, A. J. Austin, R. Cammi, C. Pomelli, J. W. Ochterski, R. L. Martin, K. Morokuma, V. G. Zakrzewski, G. A. Voth, P. Salvador, J. J. Dannenberg, S. Dapprich, A. D. Daniels, O. Farkas, J. B. Foresman, J. V. Ortiz, J. Cioslowski, and D. J. Fox, Gaussian, Inc., Wallingford CT, 2013.)
(16) Ai, J. Broadwater, J. A., Loehr, T. M., Sanders-Loehr, J., Fox, B. G. **1997**, *J. Biol. Inorg. Chem. 2*, 37-35. 16) Kurtz, D. M. Jr., Shriver, D. F. Klotz, I. M. **1977**, *Coord. Chem. Rev. 24*, 145-178. 17) Lu, S., Sazinsky, M. H., Whittaker, J. W., Lippard, S. J., Moënne-Loccoz, P. **2005**, *J. Am. Chem. Soc. 127*, 4148-4149